EUROPEAN COMMISSION
DIRECTORATE-GENERAL
Joint Research Centre

Realistic multiannual simulations of the coupled North Sea and Baltic Sea system using the GETM model.

Adolf Stips, Karsten Bolding, Hans Burchard,
Samuel Djavidnia, Elisaveta Peneva

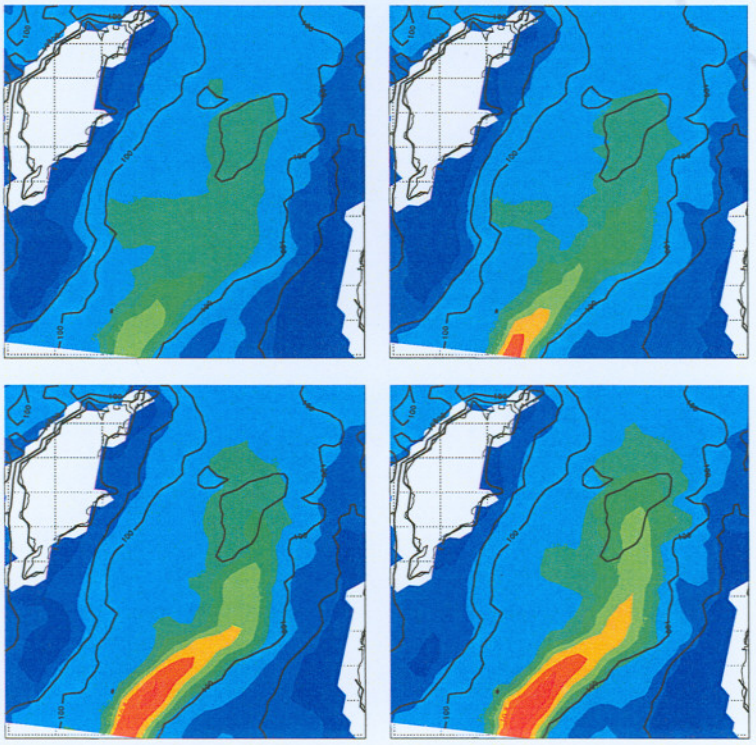

2005 EUR 21503 EN

Realistic multiannual simulations of the coupled North Sea and Baltic Sea system using the GETM model.

Adolf Stips[1], Karsten Bolding[2] Hans Burchard[3], Samuel Djavidnia[1], Elisaveta Peneva[1]

(1) CEC Joint Research Centre, Institute for Environment and Sustainability, I-21020 Ispra(VA), Italy
(2) Bolding & Burchard Hydrodynamics GbR, Strandgyden 25, DK 5466 Asperup, Denmark
(3) Institute for Baltic Sea Research, Universität Rostock, Seestrasse 15, D-18119 Rostock, Germany

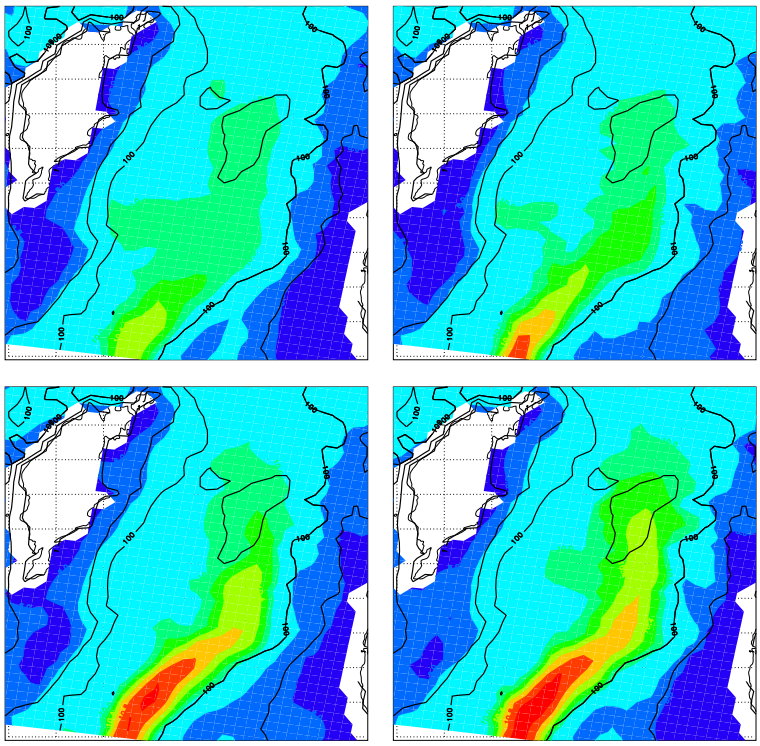

EUR 21503 EN

Printed in Italy

Abstract

Abstract: This report presents a brief summary of modelling work done for the North Sea/Baltic Sea area within the institutional action ECOMAR (Monitoring and assessment of marine ecosystems) at the Joint Research Centre (JRC). First the underlying model equations are briefly recalled. Then different model setups for the coupled North Sea – Baltic Sea system using the General Estuary Transport Model (GETM) are described. The simulation of the North Sea with a very coarse 20 km grid, was used as base study to assess the model performance. Results from the very coarse run are compared to measured data, at selected stations. Simulated Sea Surface Temperature (SST) is confronted with SST observed by satellites. More detailed multi-annual simulations were done using a coarse 6 × 6 nm grid and and fine 3 × 3 nm grid. Selected results from different applications are finally presented. This concerns specifically simulations of the Sea Surface Temperature, the inflow dynamics at the Danish Straits, as well as salt water inflows into the central Baltic proper. Many important known features of these seas are sufficiently well reproduced by the existing model setup, so that data from the simulations can be used for ecological assessments. This is imporant as data described in this study form the basis for the physical indicator development at the ECOMAR action. Nevertheless, there is still room for further improvements and for addition of new model features.

Key words: 3D-modelling – Baltic Sea – North Sea – Sea Surface Temperature – Salt water inflow – Indicator development

Contents

1 Introduction and aim of the present study

In this report we will describe the model setup and selected results of the General Estuary Transport Model (GETM) applied to the coupled North Sea and Baltic Sea.

1.1 Introduction

There are many existing numerical models for the North Sea, already less for the Baltic Sea, but only a very few for the coupled domain North Sea – Baltic Sea. Many of them are used for climatological studies, see e. g. Meier (2001) or Schrum et al. (2000). Others concentrate on the circulation, see e. g. Lehmann (1995) or the sea ice dynamics, see e. g. Omstedt et al. (1994) and Omstedt and Nyberg (1994). There are also several high-resolution regional models as for the southwestern Baltic Sea (Schmidt et al. (1998)) or the Skagerrak and Kattegat region (Funkquist and Kleine (1995)) or the western Baltic Sea (Meier (2000)). Several operational models exist for the Baltic and the North Sea such as the BSH model (Kleine (1994)) and the HIROMB model (Funkquist and Kleine (2002)).

All these models have in common that they use fixed so-called geopotential coordinates which introduce steps in the bottom bathymetry when they intersect with the bottom. There are certain problems associated with this approach such as the bad representation of dense near-bottom currents, see Beckmann and Döscher (1997)). Furthermore, the height of the near-surface layer is limited by the tidal range which is very restrictive when the full North Sea is included into the model domain. Thus, shallow sills like the Darss Sill will only be resolved by a few grid boxes in the vertical. Bathymetry-fitted coordinates such as the general vertical coordinates used in GETM do not have this disadvantage. However, also these coordinates have certain other drawbacks such as the pressure-gradient error, see e.g. Haney (1991). One clear advantage of the general vertical coordinates is their great flexibility which allows for hybrid solutions such as between geopotential and σ coordinates (see Beckers (1991), Gerdes (1993), Burchard and Petersen (1997)) and between geopotential, σ and isopycnal coordinates, see the recent development of the MICOM model by Bleck (2002).

Thus, the use of a general vertical coordinates model such as GETM is advantageous here, especially since for test simulations also geopotential coordinates could be retrieved. Other reasons for using GETM are its ability of using curvilinear grids, its high-resolution monotone advection schemes and its coupling to the turbulence module of the General Ocean Turbulence Model (GOTM,

see Burchard et al. (1999) and `http://www.gotm.net`).

1.2 Objective of the study

Multi-annual simulations of European Regional Seas are the basis for the work done in the ECOMAR action at the Inland and Marine waters (IMW) unit of the Joint Research Centre (JRC). This work is done for assessing water quality in European coastal waters using homogenised tools and methods. Nevertheless the correct understanding of the underlying hydrodynamic processes is a necessary prerequisite for doing such assessments. Many different models are not only used for the same region, but also for simulating the different European Seas. Therefore a further intention of the modelling work in the ECOMAR action is to produce comparable results for the different regions, by applying the same model to the different regions. As the first application example the North Sea and later on the coupled North Sea Baltic Sea system were selected. Results of this work will be presented in this report. This modelling exercise has already helped to assess environmental disasters, as demonstrated in the HELCOM (Helsinki Commission) report (Aertebjerg et al. (2003)) on the oxygen depletion event in the Danish Straits.

In late summer 2002 an extended and long lasting oxygen depletion event was observed in the entrance area to the Baltic (e.g. Kattegat, Sound and Belt Sea). By investigating the physical conditions, wind forcing, vertical mixing and horizontal water exchange during the year 2002 we could analyse the physical factors contributing to this strong depletion. Based on 3D hydrodynamical modelling, we examined further the horizontal and vertical exchange of water masses in the Baltic entrance area. This showed that the bottom water from July to October generally stagnated, because no inflow of oxygen rich water occurred and also the vertical stratification was strong and henceforth overall mixing was small. Therefore this unusual small mixing in the Kattegat and Belt Sea area could essentially contribute to the development of the most severe, widespread and lasting observed oxygen depletion event. We consider this study done in an HELCOM ad-hoc group of scientists from different countries, as a very good demonstration for a practical application of numerical hydrodynamic modelling to understand environmental problems

Different model setups for the coupled North Sea – Baltic Sea system using the GETM are described. First the underlying model equations are briefly recalled. The simulation of the North Sea with a very coarse 20 km grid, was used as base study to assess the model performance. More detailed multi-annual simulations were done using a coarse 6 nm$\times$ 6 nm grid and and fine 3 nm $\times$ 3 nm grid. Selected results from different applications are finally presented. This concerns specifically simulations of the Sea Surface Temperature, the

inflow dynamics at the Danish Straits, as well as salt water inflows into the central Baltic proper. Data described in this study form the basis for the physical indicator development and calculation at the ECOMAR action.

2 General model equations

This section gives a short introduction to the GETM model equations, for specific details see Burchard and Bolding (2002).

2.1 Three-dimensional momentum equations

GETM solves the three-dimensional hydrostatic equations of motion applying the Boussinesq approximation and the eddy viscosity assumption (Bryan (1969), Cox (1984), Blumberg and Mellor (1987), Haidvogel and Beckmann (1999), Kantha and Clayson (2000)).

In the flux form, the dynamic equations of motion for the horizontal velocity components can be written in Cartesian coordinates as:

$$\begin{aligned}
&\partial_t u + \partial_x(u^2) + \partial_y(uv) - \partial_x\left(2A_h^M\partial_x u\right)\\
&\\
&-\partial_y\left(A_h^M(\partial_y u + \partial_x v)\right) - fv - \int_z^\zeta \partial_x b\,dz' \\
&\\
&+\partial_z(uw) - \partial_z\left((\nu_t+\nu)\partial_z u\right) = -g\partial_x\left(g\zeta + \frac{1}{\rho_0}p_0\right),
\end{aligned} \tag{1}$$

$$\begin{aligned}
&\partial_t v + \partial_x(vu) + \partial_y(v^2) - \partial_y\left(2A_h^M\partial_y v\right)\\
&\\
&-\partial_x\left(A_h^M(\partial_y u + \partial_x v)\right) + fu - \int_z^\zeta \partial_x b\,dz' \\
&\\
&+\partial_z(vw) - \partial_z\left((\nu_t+\nu)\partial_z v\right) = -g\partial_y\left(g\zeta + \frac{1}{\rho_0}p_0\right)\zeta.
\end{aligned} \tag{2}$$

The vertical velocity is given by the continuity equation:

$$\partial_x u + \partial_y v + \partial_z w = 0. \tag{3}$$

Here, u, v and w are the ensemble averaged velocity components with respect to the x, y and z direction, respectively. The vertical coordinate z ranges from the bottom $-H(x,y)$ to the surface $\zeta(t,x,y)$ with t denoting time. ν_t is the vertical eddy viscosity, ν the kinematic viscosity, f the Coriolis parameter, p_0 is the atmospheric pressure at sea level and g is the gravitational acceleration.

The horizontal mixing is parameterised by terms containing the horizontal eddy viscosity A_h^M, see Blumberg and Mellor (1987). The buoyancy b is defined as

$$b = -g\frac{\rho - \rho_0}{\rho_0} \tag{4}$$

with the density ρ and a reference density ρ_0. The last term on the left hand sides of equations (1) and (2) are the internal (due to density gradients) and the terms on the right hand sides are the external (due to surface slopes and atmospheric pressure variations) pressure gradients. In the latter, the deviation of surface density from reference density is neglected (see Burchard and Petersen (1997)). The derivation of equations (1) - (3) has been shown in numerous publications, see e.g. Pedlosky (1987), Haidvogel and Beckmann (1999), Burchard (2002).

The equation of state for seawater (see Fofonoff and Millard (1983)) is used to calculate density as a function of salinity, temperature and pressure.

In hydrostatic 3D models, the vertical velocity is calculated by means of equation (3). Due to this, mass conservation and free surface elevation can easily be obtained.

2.2 Kinematic boundary conditions and surface elevation equation

At the surface and at the bottom, kinematic boundary conditions result from the requirement that the particles at the boundaries are moving along these boundaries:

$$w = \partial_t\zeta + u\partial_x\zeta + v\partial_y\zeta \qquad \text{for } z = \zeta, \tag{5}$$

$$w = -u\partial_x H - v\partial_y H \qquad \text{for } z = -H. \tag{6}$$

2.3 Dynamic boundary conditions

At the bottom boundaries, no-slip conditions are prescribed for the horizontal velocity components:

$$u = 0, \quad v = 0. \tag{7}$$

With (6), also $w = 0$ holds at the bottom. It should be noted, that the bottom boundary condition (7) is generally not directly used in numerical ocean models, since the near-bottom values of the horizontal velocity components

are not located at the bed, but half a grid box above it. Instead, a logarithmic velocity profile is assumed in the bottom layer, leading to a quadratic friction law.

At the surface, the dynamic boundary conditions read:

$$\begin{aligned}(\nu_t + \nu)\partial_z u &= \tau_s^x, \\ (\nu_t + \nu)\partial_z v &= \tau_s^y,\end{aligned} \tag{8}$$

The surface stresses (normalised by the reference density) τ_s^x and τ_s^y are calculated as functions of wind speed, wind direction, surface roughness etc.

2.4 Lateral boundary conditions

Boundary conditions at closed and open boundaries will be treated differently. At closed boundaries, the flow must be parallel to the boundary.

For an eastern or a western closed boundary this has the consequence that $u = 0$ and, equivalently, for a southern or a northern closed boundary it follows that $v = 0$.

At open boundaries, the velocity gradients across the boundary must vanish. For an eastern or a western open boundary this has the consequence that $\partial_x u = \partial_x v = 0$ and, equivalently, for a southern or a northern open boundary it follows that $\partial_y u = \partial_y v = 0$.

At so-called forced open boundaries, the sea surface elevation ζ is prescribed. This is here done at the western, eastern and northern open boundary.

2.5 Transport equations for temperature and salinity

The two most important tracer equations are the transport equations for potential temperature T in °C and salinity S in PSU (practical salinity units):

$$\begin{aligned}&\partial_t T + \partial_x(uT) + \partial_y(vT) + \partial_z(wT) - \partial_z(\nu_t'\partial_z T) \\ &\quad -\partial_x(A_h^T\partial_x T) - \partial_y(A_h^T\partial_y T) = \frac{\partial_z I}{c_p'\rho_0},\end{aligned} \tag{9}$$

$$\partial_t S + \partial_x(uS) + \partial_y(vS) + \partial_z(wS) - \partial_z(\nu_t' \partial_z S)$$
$$-\partial_x(A_h^T \partial_x S) - \partial_y(A_h^T \partial_y S) = 0. \tag{10}$$

The term on the right hand side of the temperature equation (9) is for absorption of solar radiation with the solar radiation at depth z, I, and the specific heat capacity of water, c_p'. According to Paulson and Simpson (1977) the radiation I in the upper water column may be parameterised by

$$I(z) = I_0 \left(a e^{-\eta_1 z} + (1-a) e^{-\eta_2 z} \right). \tag{11}$$

Here, I_0 is the albedo corrected radiation normal to the sea surface. The weighting parameter a and the attenuation lengths for the longer and the shorter fraction of the short-wave radiation, η_1 and η_2, respectively, depend on the turbidity of the water. Jerlov (1968) defined 6 different classes of water from which Paulson and Simpson (1977) calculated weighting parameter a and attenuation coefficients η_1 and η_2.

At the surface, flux boundary conditions for T and S have to be prescribed. For the potential temperature, it is of the following form:

$$\nu_t' \partial_z T = \frac{Q_s + Q_l + Q_b}{c_p' \rho_0}, \qquad \text{for } z = \zeta, \tag{12}$$

with the sensible heat flux, Q_s, the latent heat flux, Q_l and the long wave back radiation, Q_b. Bulk formulae prescribed by the NOMADS2 consortium (Proctor et al. (2002)) for calculating the momentum and heat surface fluxes due to air-sea interactions were used for the very coarse simulation of the North Sea. For all other simulations we applied the Kondo (1975) bulk formulae.

For the surface freshwater flux, which defines the salinity flux, the difference between evaporation Q_E (from bulk formulae) and precipitation Q_P (from observations or atmospheric models) is calculated:

$$\nu_t' \partial_z S = \frac{S(Q_E - Q_P)}{\rho_0(0)}, \qquad \text{for } z = \zeta, \tag{13}$$

where $\rho_0(0)$ is the density of freshwater at sea surface temperature. Heat and salinity fluxes at the bottom are set to zero.

The eddy viscosity ν_t (for momentum) and eddy diffusivity ν'_t (for tracers) need to be parameterised by means of turbulence models. Such models may range from simple algebraic prescription of profiles of ν_t and ν'_t (see Perrels and Karelse (1982)), via zero-, one, or two-equation models (see e.g. Luyten et al. (1996)) to full Reynolds stress closure models (see e.g. Launder et al. (1975)). In GETM, a compromise between accuracy and computational effort is made in such a way, that usually two-equation models are used.

The turbulence module of the Public Domain water column model GOTM (General Ocean Turbulence Model, see `http://www.gotm.net`) which has been developed by Burchard et al. (1999) is implemented into GETM. This allows for great flexibility in the choice of the turbulence model and guarantees that a well-tested state-of-the-art turbulence model is always at hand inside GETM.

The features of GOTM have been extensively reported in Burchard (2002) and the citations therein. Various comparative calculations with in-situ turbulence measurements have been carried out with GOTM, which gives some confidence into the model, see e.g. Bolding et al. (2002), Burchard et al. (2002), Simpson et al. (2002) and Stips et al. (2002).

GOTM has various options for turbulence models, but only some of them have been proven to give reasonable results for vertical exchange. The research for improving turbulence models is still ongoing. Presently, better parameterisations for surface wave activity and internal wave activity are under development.

So far, the best experience inside GOTM has been made with two-equation models such as the k-ε (see Launder and Spalding (1972), Rodi (1980)) and the Mellor-Yamada model (Mellor and Yamada (1974), Mellor and Yamada (1982) and Burchard (2001a)), both being realisations of the recently developed generic two-equation model by Umlauf and Burchard (2003).

The basic one-dimensional form of the k-ε model is the following (see Burchard et al. (2002)):

$$\partial_t k - \partial_z \left(\left(\nu + \frac{\nu_t}{\sigma_k} \right) \partial_z k \right) = P + B - \varepsilon, \tag{14}$$

$$\partial_t \varepsilon - \partial_z \left(\left(\nu + \frac{\nu_t}{\sigma_\varepsilon} \right) \partial_z \varepsilon \right) = \frac{\varepsilon}{k} (c_{1\varepsilon} P + c_{3\varepsilon} B - c_{2\varepsilon} \varepsilon), \tag{15}$$

with the equation for turbulent kinetic energy, (14), and for its dissipation rate ε, (15). σ_k and σ_ε denote turbulent Schmidt numbers for vertical diffusion

of k and ε, respectively, and P and B are shear and buoyancy production, respectively with:

$$P = \nu_t \left((\partial_z u)^2 + (\partial_z v)^2 \right), \qquad B = -\nu'_t \partial_z b, \tag{16}$$

and $c_{1\varepsilon}$, $c_{2\varepsilon}$, and $c_{3\varepsilon}$ are empirical parameters.

Suitable bottom and surface boundary conditions for k and ε can be derived from the law of the wall, although modifications are needed near the surface due to breaking of surface waves (see Craig and Banner (1994), Craig (1996), Burchard (2001b)).

The three turbulent parameters k, ε and L are interrelated through:

$$L = c_L \frac{k^{3/2}}{\varepsilon} \tag{17}$$

with the empirical parameter c_L.

From k and ε, the eddy viscosity and diffusivity can finally be calculated by the following relation:

$$\nu_t = c_\mu \frac{k^2}{\varepsilon}, \qquad \nu'_t = c'_\mu \frac{k^2}{\varepsilon}. \tag{18}$$

Here, c_μ and c'_μ are so-called stability functions usually depending on shear, stratification and turbulent time scale, $\tau = k/\varepsilon$.

Various sets of stability functions, which contain second-moment closure assumptions have been suggested. The most successful in terms of comparison to laboratory and field data seems to be the closure introduced by Canuto et al. (2001), which are used in this study.

The turbulence model is coupled to the hydrodynamic model via the turbulence production terms P and B as input and the eddy viscosity and diffusivity ν_t and ν'_t as output. Furthermore, surface and bottom roughness lengths are needed for the boundary conditions inside the turbulence model. Finally, the three-dimensional model needs to store two quantities out of k, ε and L since GOTM is a one-dimensional model which has to read in the "old" values of k, ε and L for each horizontal position. Advective transports of turbulent quantities are neglected here.

3 Results for very coarse North Sea simulations

Results of the 1 year realistic model run for 1989 using the very coarse resolution GETM setup for the North Sea are presented and compared to North Sea project data and to satellite observations. An identical setup was used for investigating the influence of 3 different advection schemes, namely the upstream scheme (GETM-UP), and the total variance diminishing schemes using the superbee delimiter (GETM-SU) and the ultimate quickest delimiter (GETM-QU). Some of the results are compared to simulations done by Thomas Pohlmann using the HAMSOM (Hamburg Shelf Ocean Model) for the NOMADS2 scenario. A short description of the selected setup is given before showing and discussing the results of this very coarse resolution experiment. A more detailed description of the NOMADS2 comparison study in general can be found in Delhez et al. (2004), while for more information concerning the GETM application to the NOMADS2 test case see Stips et al. (2004).

3.1 Setup very coarse resolution experiment

The turbulence scheme of GETM is chosen via the GOTM turbulence model. In this study we used the standard k-ε turbulence closure, without imposing a length limitation or background vertical diffusivity. GETM uses different time steps for the internal (macro time steps) and the external mode (micro time steps). The chosen micro time step for this setup is 60 s, the split factor is 30, which gives a macro time step of 1800 s. No background horizontal diffusion was applied. It could be argued, that this is not the most appropriate approach, because of the used large grid size and the therefore unresolved subgrid mesoscale mixing. But as one focus was to look at the influence of different advection schemes, we avoided the introduction of horizontal diffusion, as this could have masked the differences between the performed simulations. The imposed boundary conditions for temperature and salinity are relaxed to the model values using a 5 point sponge layer. To better resolve the shallow parts of the North Sea, we decided to use general vertical coordinates with a slight zooming towards the surface and the bottom. The surface layer thickness has been chosen to be two metres overall.

3.1.1 Model domain

The model domain was chosen to coincide exactly with the setup of the HAMSOM model for the NOMADS2 model comparison study. It covers the North Sea from the channel to 61,5^o N, with a horizontal resolution of about 20 km. The longitudinal grid size is $\Delta x = 20'$ and the latitudinal grid size is $\Delta y = 12'$.

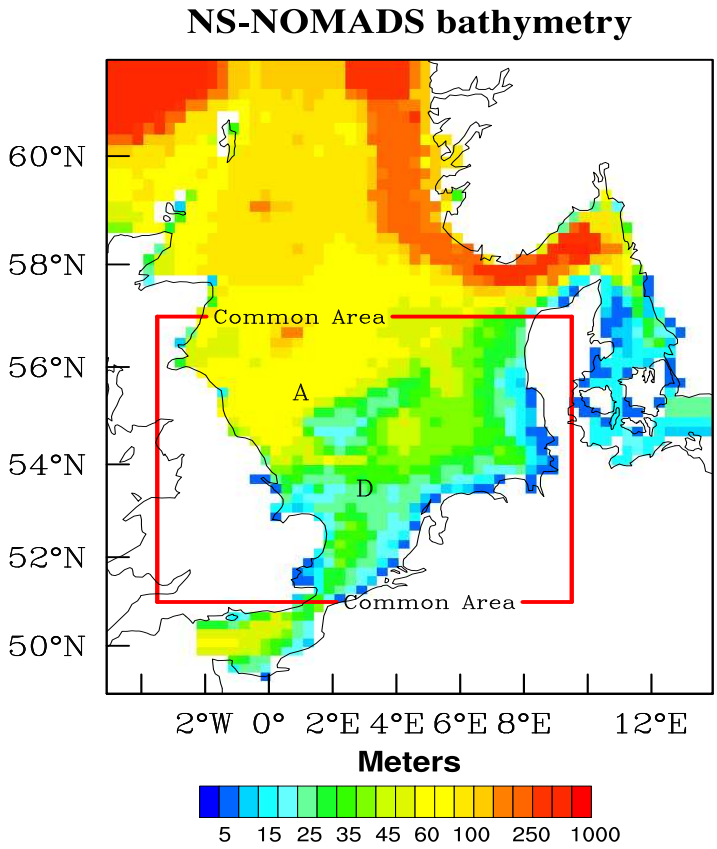

Fig. 1. Model bathymetry (depth in meters) for the North Sea area. The specified area "Common Area" is indicated by a red box. The selected stations from the North Sea project are denoted by A (stratified) and D (mixed).

The used bathymetry is shown in figure 1. The grid size for the model is $58*65*19$ $(x*y*z)$ points.

3.1.2 Meteorological forcing

The simulation period is November 1, 1988 to October 31, 1989. The realistic meteorological forcing used for GETM, was provided from the UK Meteorological Office. Space and time varying variables such as wind velocity vector, air pressure, air temperature, relative humidity and cloudiness have been used to calculate surface heat and momentum fluxes. Bulk heat flux formulations, as prescribed by the NOMADS2 consortium had been applied. The 3 hourly meteorological data were interpolated onto the model grid.

3.1.3 Initial and boundary conditions

For all different runs the same initial conditions were applied for water elevation, salinity and temperature. Consistent boundary values for water elevation, salinity and temperature for the one-year realistic simulation were used. The time frequency of the tidal data is hourly. Salinity and temperature are given at monthly intervals. These data sets are identical to the NOMADS2 initial and boundary data set. For river runoff and Baltic inflow, monthly mean values were used. The temperature of the fresh water inflow was assumed to be the ambient temperature.

3.2 Comparison to North Sea project observations

In this section the model data are compared to observational data from a stratified and a well mixed station (see Lowry et al. (1992)). These stations had been selected already by the NOMADS2 (North Sea Model Comparison Study) consortium in order to compare model results to CTD data. Furtheron we will refer to the results of the HAMSOM (Hamburg Shelf Ocean Model, Backhaus (1985)) NOMADS2 run for the same stations.

3.2.1 Stratified station temperature

The vertical temperature field during the NOMADS2 annual simulation at a selected Station A (55.5^o N, 0.9^o E, 68 m depth, see figure 1) is presented in figure 2. At this station the water column is mixed during the winter and stratified in the summer. In the different model simulations the annual cycle of stratification and mixing is well reproduced. The results of the GETM-UP run (not shown) are very similar to the HAMSOM results.

The vertical stratification during summer is more pronounced when using higher order advection schemes, especially the thermocline is nearer to the surface and sharper, which is in better agreement with the available measurements. The surface temperatures are in good agreement with the measurements, but the water at the bottom warms up too early and too quickly.

The maximum temperature (in ^oC) reaches 15.35 in HAMSOM, 15.23 GETM-UP and 16.51 GETM-SU, 16.53 in GETM-SU2, 16.48 in GETM-QU and 16.40 in GETM-QU2. The maximum temperature from the CTD data was 15.84 ^oC, but because of the low sampling frequency the real maximum temperature might have been missed in the measurements.

Comparing the model results to monthly measurements taken during that year at station A, we find that the evolution of the thermocline begins at around day

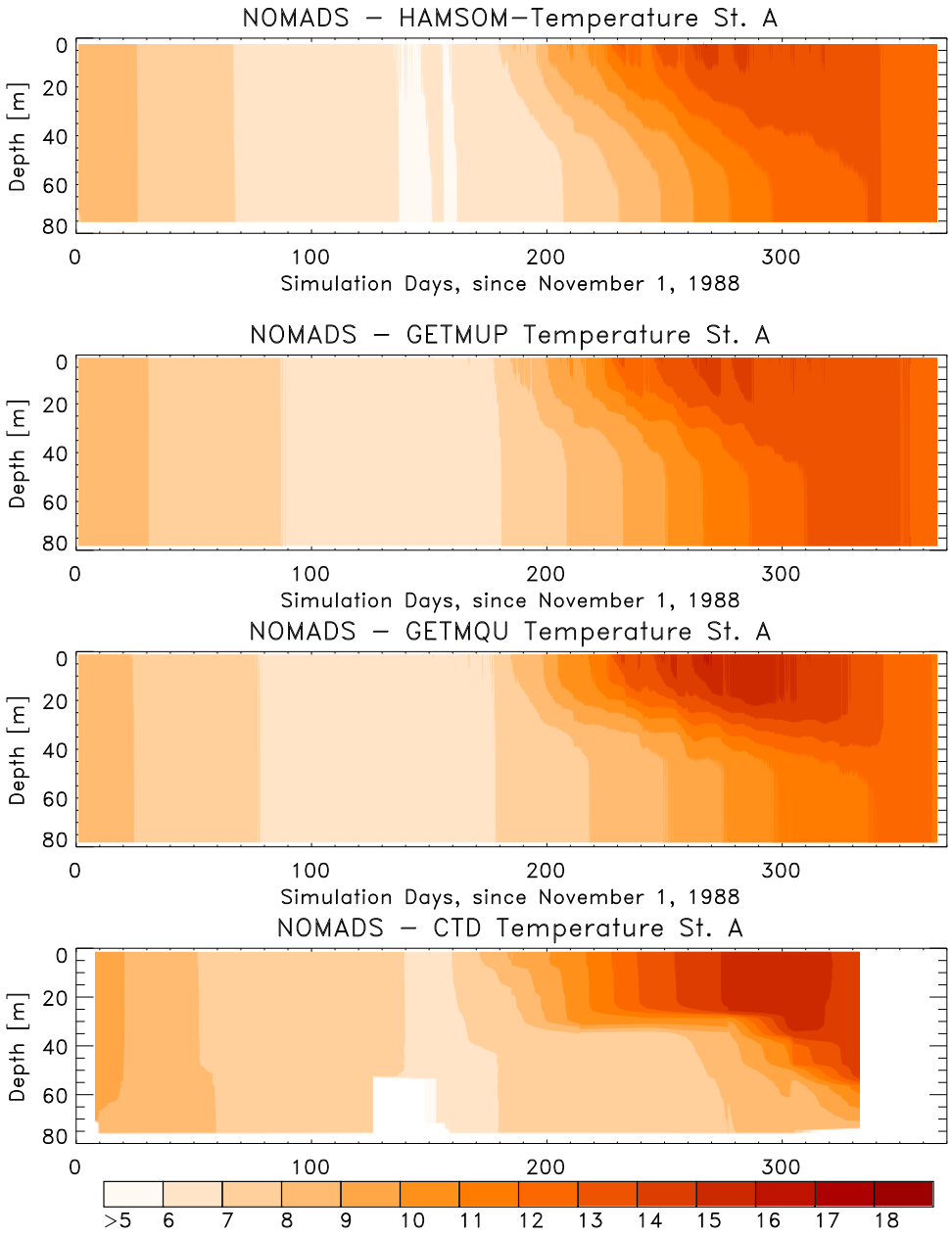

Fig. 2. Temporal evolvement of the temperature fields at the NOMADS2 station A (stratified) for different advection schemes. The lower most panel shows the measurements from the North Sea project.

180, in accordance with the measurements. The low sampling frequency of the measurements does not allow a precise determination of this time point. The best agreement with the measurements is found in the GETM-QU simulations.

The strength of the stratification can be characterised by the temperature difference between the upper 5 m and the bottom most 5 m. This so called thermal stratification for station A is displayed in figure 3. The results for

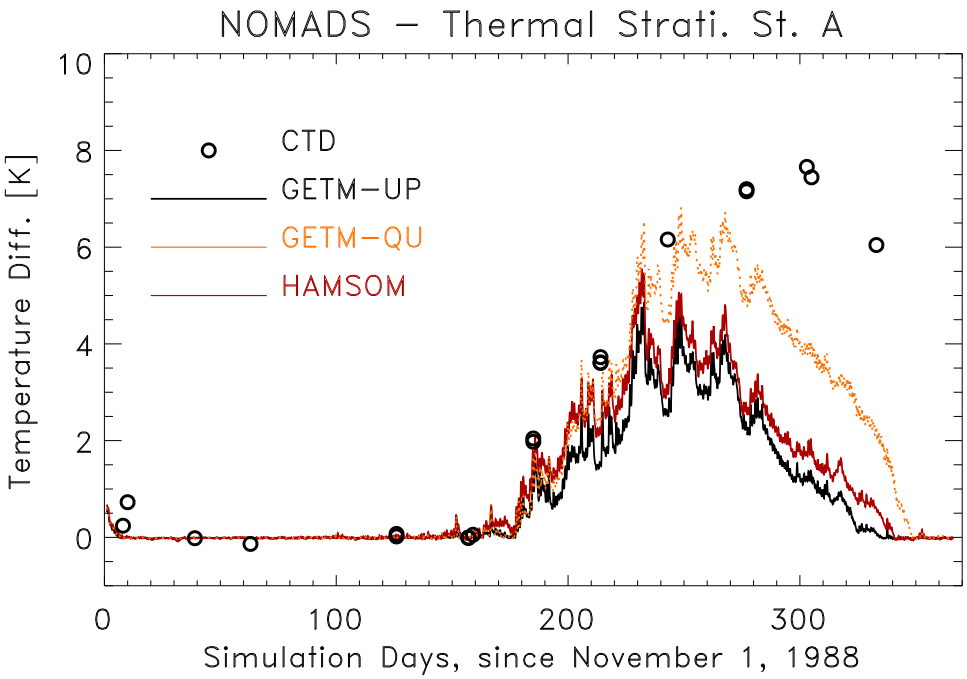

Fig. 3. Thermal stratification at station A (stratified), shown are results for the two models and different advection schemes. The open circles are the North Sea project data (monthly cruises).

HAMSOM and GETM-UP agree quite well. Both models are well mixed until day 150, stratified between day 150 and day 340 and mixed again after day 340. HAMSOM shows a slightly larger temperature difference during the stratified phase of about 0.1 K to 0.3 K more than GETM-UP. This result changes dramatically if we compare to the GETM-SU and GETM-QU output. Now during the re-stratification period between day 150 and day 230 GETM-QU and HAMSOM agree very good, but between day 230 and day 350 GETM-SU/GETM-QU exceeds HAMSOM by about 2 to 3 K, in better agreement with the CTD data. The maximum temperature difference between bottom and surface is 4.95 K for GETM-UP, 5.58 K for HAMSOM, 7.55 K for GETM-SU 6.86 K for GETM-QU. The measurements gave a maximum temperature difference of 7.7 K.

3.2.2 Stratified station salinity

The small salinity variability of less than 1 PSU at the selected NOMADS2 stations, makes the good simulation of salinity a challenging task. The results obtained from HAMSOM, from different GETM runs and from the North Sea project data are detailed in figure 4. The largest differences are in the order of 0.06-0.08 PSU.

It can be seen that the differences between the model and the measurements

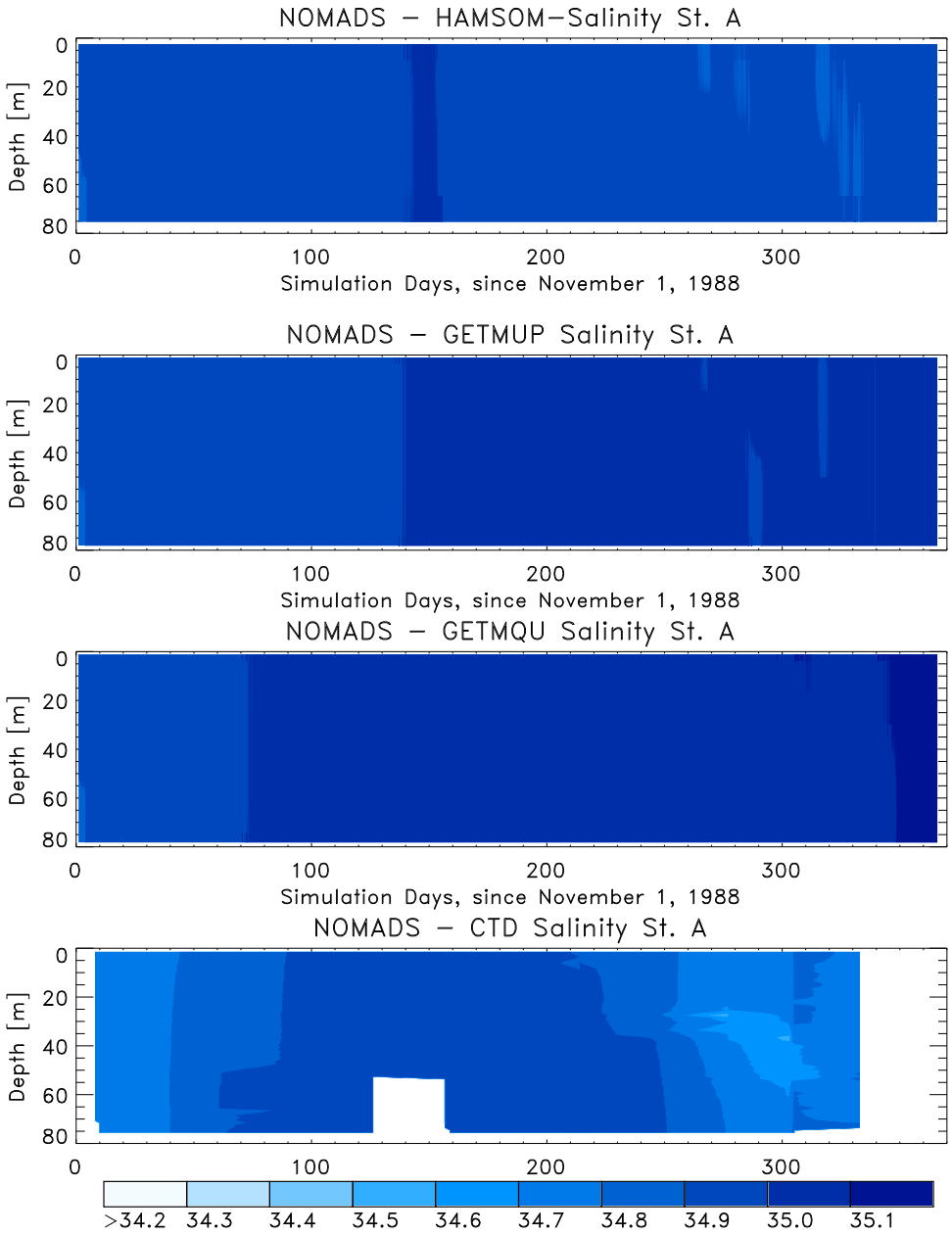

Fig. 4. Temporal evolvement of the salinity fields at the NOMADS2 station A (stratified) for the different advection schemes and measurement data from the North Sea project.

in salinity are rather small during most of the year, except at the end of the simulation period.

Further to this we investigated the salinity difference between the uppermost 5 m and the bottom most 5 m and compared them to CTD data, see figure 5. This figure reveals that the realistic simulation of salinity in the North Sea is more difficult to achieve than the hind-casting of temperature. The

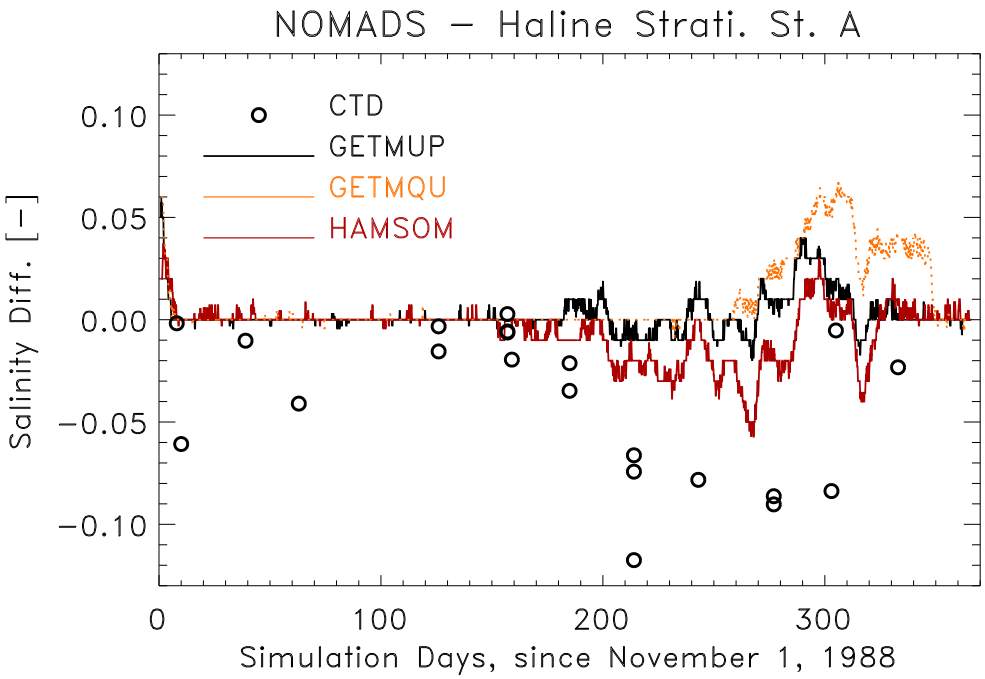

Fig. 5. Haline stratification at station A (stratified), shown are results for the different used advection schemes. The open circles are the North Sea project data (monthly cruises).

measurements indicate that during most of the year the salinity stratification is either stable or neutral, whereas all the simulations show during summer and especially in autumn some periods of instable saline stratification. In this case HAMSOM gives the relative best result. From the North Sea project data, it can be seen that the saline stratification has a large short term variability. This can be inferred from the appearance of two or more circles at around the same measurement time, which represent casts from the same monthly cruise. Clearly such a short term variability cannot be reproduced, by the models, as they were forced by monthly mean values for river runoff and net precipitation.

3.2.3 Well mixed station temperature

The vertical temperature field during the NOMADS2 annual simulation at the selected Station D (53.5^o N, 3^o E, 27 m depth, see figure 1) is presented in figure 6. During most of the year the water column is well mixed, only some minor stratification appears between day 180 and day 250. The annual cycle at this station is well reproduced by all the different advection schemes. The lowest temperature in winter (around day 100) in the simulations is about 1 K less than in the measurements.

Minimum and maximum temperatures of the different model runs are given in table 3.2.3. This shows that the accuracy of the simulations is in the order

RUN Id	min. Temp.	max. Temp.
GETM-UP	5.66	17.71
GETM-SU	5.35	18.27
GETM-QU	5.44	18.07
NSP-CTD	6.02	17.84

Table 1
Minimum and maximum temperatures (in ^oC) from different model runs and CTD data at station D.

of 0.5 ^oC.

The strength of the thermal stratification at this rather mixed station D is much less compared to the stratified station A, see figure 7. The differences between the different models and advection schemes are quite small in this case. Until about day 150 of the simulation, the water column is completely mixed. Thereafter we see, that despite the NOMADS2 classification as mixed station, stratified and non-stratified periods occur alternately during the summer. This is related to the changing position of the tidal front in the North Sea and may be also related to the spring-neap tidal cycle. The North Sea project data coincide in this case quite well with the simulations.

3.2.4 Well mixed station salinity

The salinity range at the NOMADS2 station D is very limited. Therefore the correct simulation of salinity during an annual run is difficult to obtain. The contour plots of salinity are displayed in figure 8, showing the results for HAMSOM and 2 different tracer advection schemes compared to the data from the North Sea project. The agreement is less satisfactory than at the stratified station A. In this case even the better advection scheme which was used, shows less favourable results, which suggest that the unsatisfactory simulation of the salinity field is not caused by the advection scheme applied. The major reason for this behaviour might be the insufficient spatial and temporal resolution of the fresh water fluxes used.

The simulated haline stratification and the measured strength of haline stratification are of about the same order of magnitude, as can be seen from figure 9. The typical measured and simulated salinity differences are in the order of ± 0.01 PSU, showing both stable and unstable stratification. Taking into account the limited accuracy of the CTD measurements, it can be concluded that the vertical strength of stratification is rather well reproduced. Contrary to the above shown contour plot, here the results for GETM-QU agree better with the CTD data. This is probably because the absolute value of salinity cancels out, and the vertical stratification alone is better reproduced with the

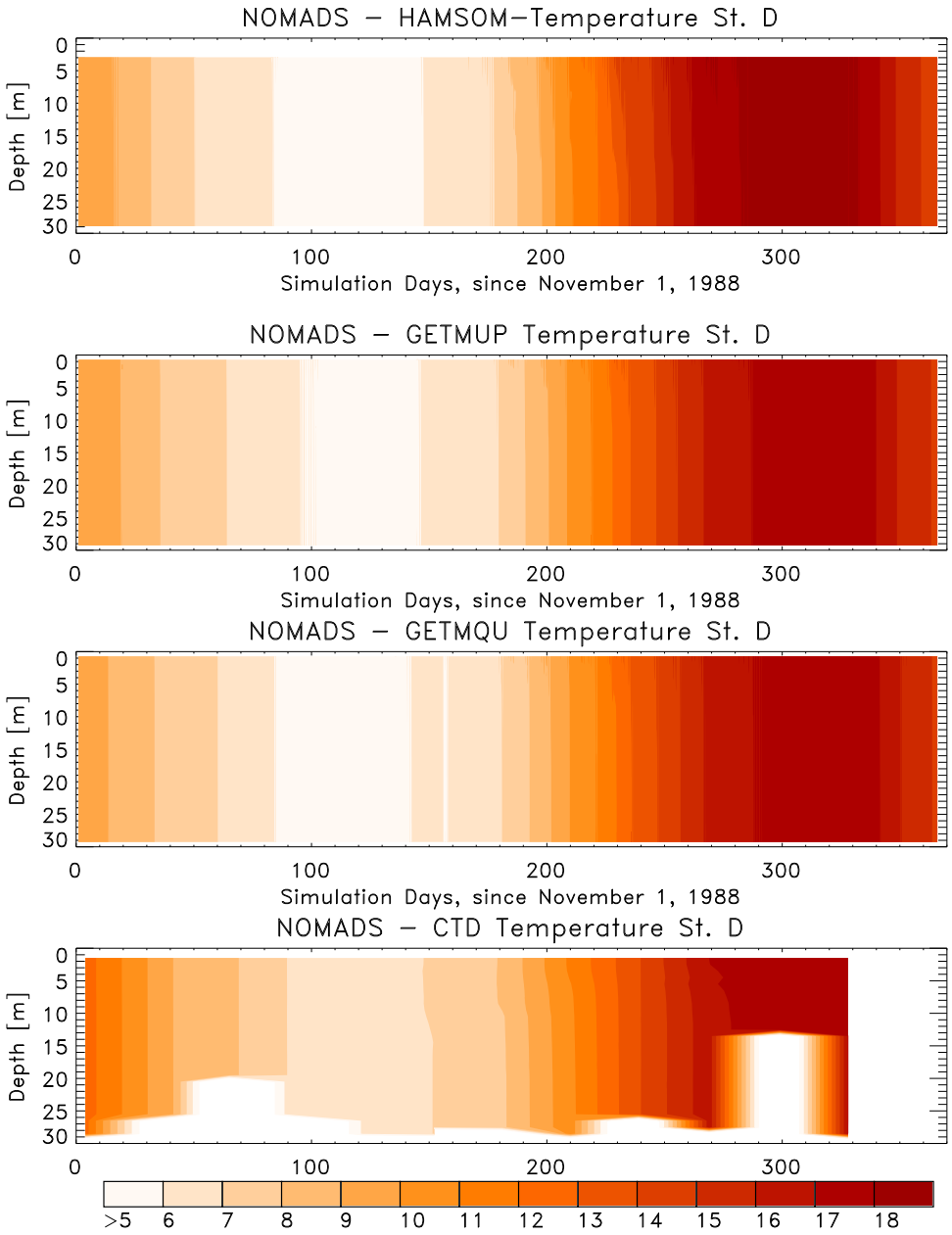

Fig. 6. Temporal evolvement of the temperature fields at the NOMADS2 station D (mixed) for different advection schemes and measurement data from the North Sea project.

help of a better advection scheme.

3.2.5 Discussion

It is not a priori clear that using an improved numerics while having the same forcing, will give results closer to the measured values. This was also

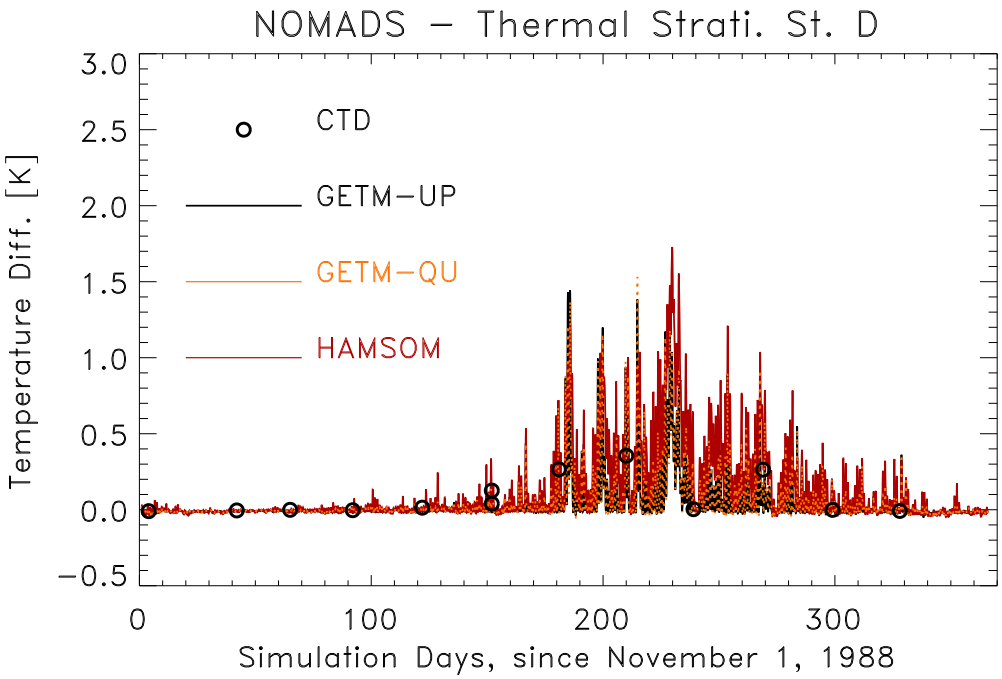

Fig. 7. Thermal stratification at NOMADS station D. Shown are results for different advection schemes and data from the North Sea project.

shown by the NOMADS2 comparison study (Proctor et al. (2002)), in which some models using advanced advection/turbulence schemes did not give significantly better results than HAMSOM. To test model results against station data, which represent instantaneous measurements at a fixed point is always a challenging task. The stations were arbitrary selected by the NOMADS2 consortium to represent contrasting dynamical behaviour during the annual simulation. The annual cycle of cooling and warming was well reproduced at both stations. This is especially true for the surface temperatures. It can be noted, that using a better turbulence closure and advection scheme within GETM will give better results, compared to HAMSOM (see figure 3). As HAMSOM was belonging to the group of the most realistic models during the NOMADS2 comparison of model to North Sea project data, this confirms that GETM is able to reproduce the temperature and salinity observations at least as well as, if not better than, the best models for the North Sea.

Less favourable was the simulation of the sharpness of the thermocline and the bottom temperature at the stratified station A. Most likely the model overestimates the vertical diffusion, which will smear out the thermocline and transports too much heat downwards. This is expressed in figures 2 and 3, where we can see that the smaller thermal stratification is mainly caused by the higher bottom temperatures. It is therefore not surprising that the temperature simulation at the well mixed station D, is reproducing the measurements very well, even when using UPSTREAM advection. In this case the

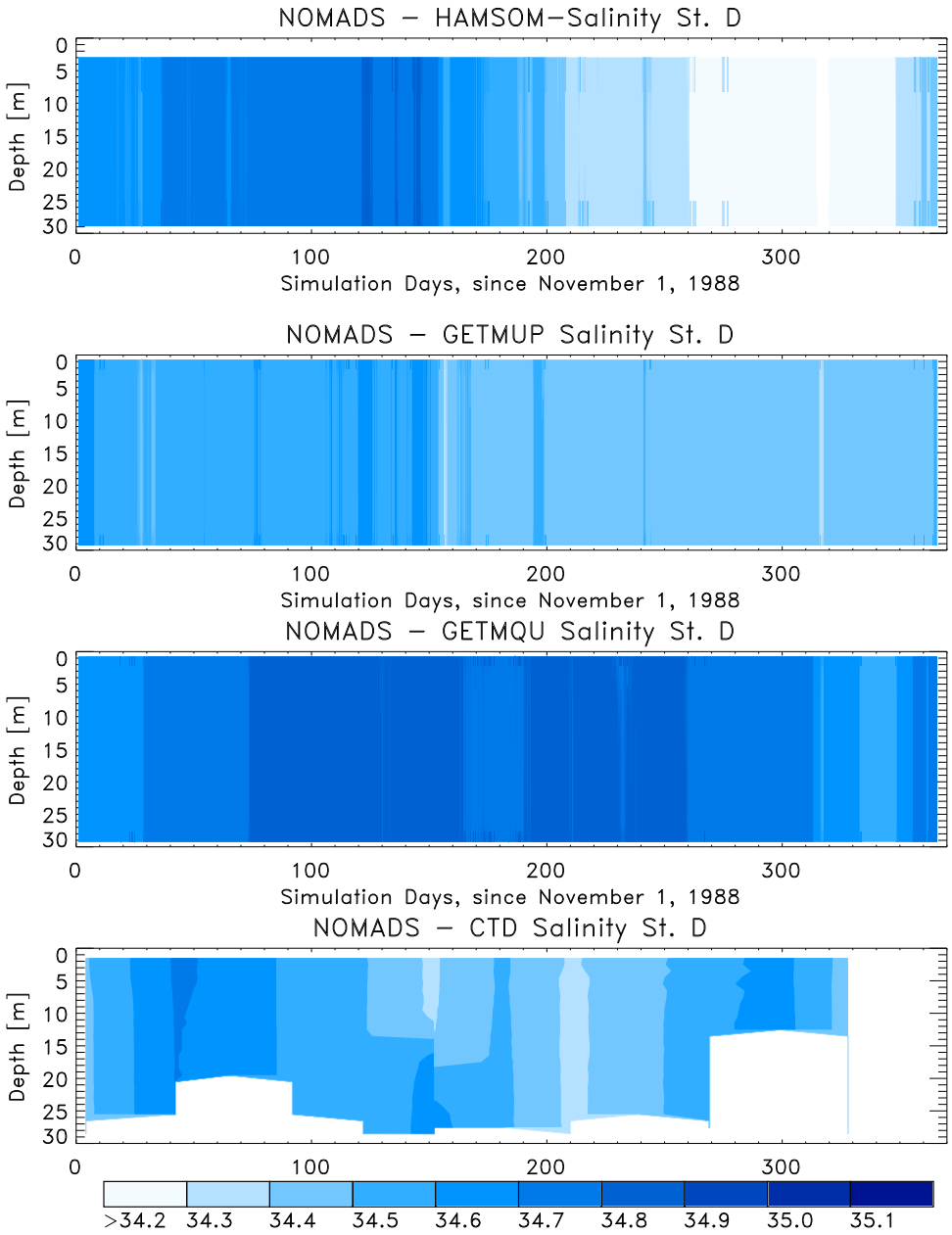

Fig. 8. Temporal evolvement of the salinity fields at the NOMADS2 station D (mixed) for the different advection schemes compared to measurements from the North Sea project.

diffusive behaviour of the UPSTREAM advection does not matter, since there are practically no vertical gradients to be diffused.

Even more difficult seems to be the prognostic treatment of salinity in the North Sea, as it is influenced by inflow of fresh water from several large rivers as well as by the inflow from less saline water from the Baltic Sea and the difference between evaporation and precipitation. Especially at station D, several

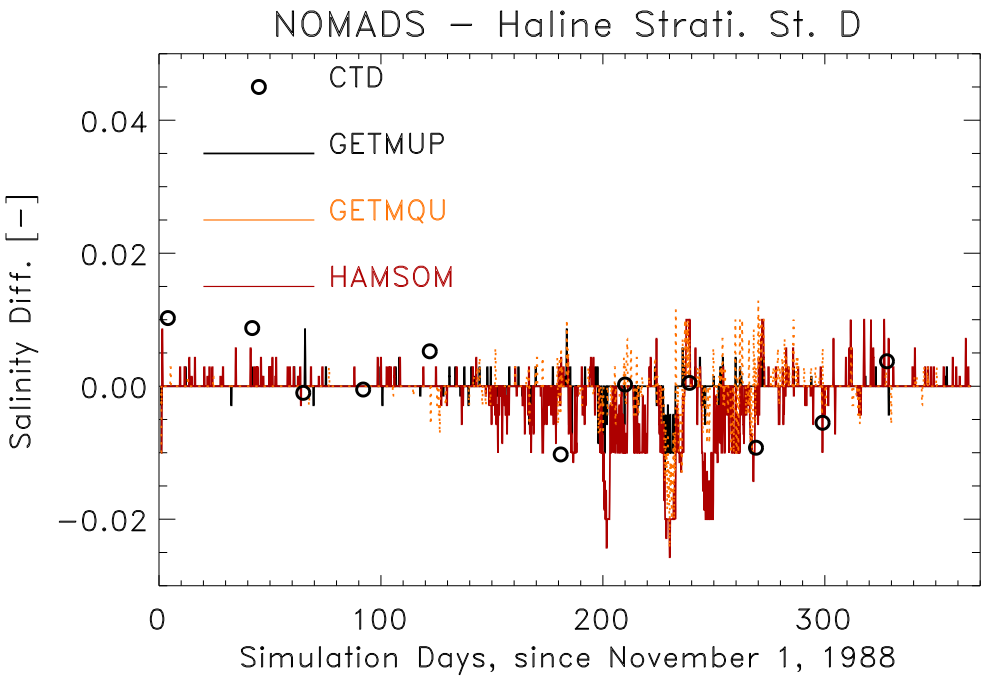

Fig. 9. Haline stratification at the well mixed station D. Shown are results for the different used advection schemes. The open circles are the North Sea project data (monthly cruises).

times less saline water bodies, probably caused by river outflow were found. These events could not be not reproduced by the model. Similar problems with the salinity simulation were reported by the NOMADS2 consortium (Proctor et al. (2002)). But it must be considered that the forcing for the fresh water fluxes was far from being optimal. Instead of using monthly mean values as done in the NOMADS2 study, at least daily fresh water fluxes must be prescribed in order to achieve a more realistic simulation of salinity. This underlines that with present day models and forcing data, we are still not capable to accurately reproduce the dynamics at an arbitrarily selected station. This has of course to do with the uncertainty of the initial and boundary conditions as well as that of the forcing data which can lead to increasing deviations from reality with time. Further to this, it must be considered that we indeed compare point like measurements to mean values from the selected grid box. In order to allow for quantitate comparisons, a sampling strategy for the measurements should be developed, which would provide real temporal and spatial averages over selected grid boxes.

3.3 Comparison to satellite observations

To compare the model's Sea Surface Temperature (SST), to satellite observations of SST, we use monthly 18 km AVHRR data from the NOAA/NASA Ocean Pathfinder satellite, see http://podaac.jpl.nasa.gov/sst. The 18 km data were chosen, since they have a similar horizontal resolution to the model setup. The accuracy of the satellite SST's is supposed to be in the order of about 0.5 K, Annan and Hargreaves (1999).

3.3.1 Mean Sea Surface Temperature

In order to investigate the annual cycle of SST, we calculated the mean SST and rms deviations in the Common Area from the monthly satellite data. The same was done for the monthly mean data of the runs GETM-UP, GETM-SU and GETM-QU. The results of these calculations are shown in figure 10. The temperature during the model initialisation was obviously too low, as the satellite SST is about 2 K higher than the modelled SST's in November 1988. During the following winter month's until April 1989 both temperatures agree to within 0.5 K. During the warming up of the North Sea from April to August 1989 the satellite SST exceeds the model SST by about 1 K, and showing finally a reversed behaviour during the cooling in autumn 1989. As can be seen by the indicated errors bars using the rms deviations, all monthly mean values fall within the distance of the rms deviation. The rms deviations vary from about 0.4 K in April/May to about 1.8 K in August/September. The SST's from all different model runs are practically the same during the winter period. During the summer GETM-SU and GETM-QU are still equal, whereas GETM-UP is about 0.5 K cooler.

3.3.2 Spatial Variability of SST

The composite mean SST for the AVHRR data in January 1989 and February 1989, are shown in figure 11 together with the model results. The respective data for the summer months July and August 1989 are shown in figure 12. These figures show the overall model domain, but the focus for the comparisons shall remain on the Common Area, indicated by the red lines. The model has some success in reproducing the large-scale features of the satellite SST during the year. This concerns the appearance of colder water in the central North Sea during winter and the general South-North temperature gradient in the southern North Sea.

The satellite images show generally more small-scale variability than the model results. The results of GETM-UP are especially smoothed compared to those from GETM-QU. This can be best seen when comparing the images from

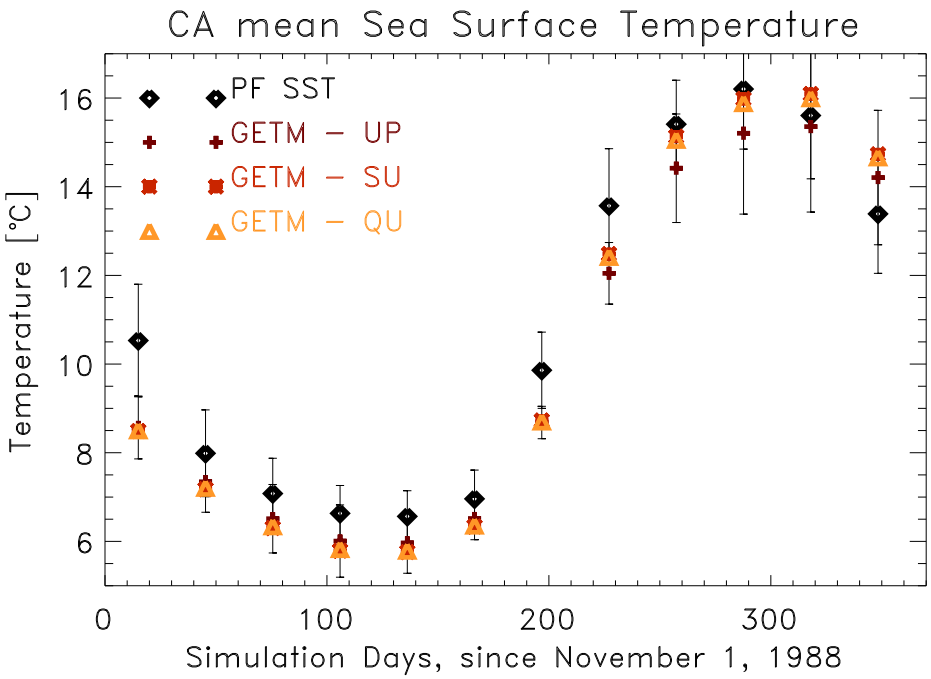

Fig. 10. Annual cycle of the monthly mean SST for the NOMADS2 Common Area region, including their rms deviations. PF SST are the satellite derived SST, whereas the other three data sets are from the different GETM runs.

August 1989 with each other. Here we can find surface temperatures of more than 18 ^oC near to the Dutch coast in the AVHRR data and GETM-QU results, but not in GETM-UP. Very cold coastal waters during January 1989 and February 1989 are more restricted to the German coastal zone, as also seen in the respective satellite data.

Compared to what is described in Holt and James (2001) we find that the seasonal dynamics in the Norwegian Trench is not that much underestimated by our model. Holt and James (2001) stated that the underestimation in their case was caused by the use of σ-coordinates, which lead to rather large layer thicknesses at the deeper parts. As we used general vertical coordinates having a quasi constant upper most layer thickness of about 2 m, this problem could be avoided in this simulation.

Clearly in this study the model results are very much dependent on the boundary conditions used, which are far from being optimal (Proctor et al. (2002)) for a realistic study, but were chosen in order to be equal for all NOMADS2 participants. In the view of this additional handicap we consider the results of the temporal spatial dynamics as satisfactory. The better resolved spatial variability, when using the same grid size for both runs, again favours the use of higher order advection schemes.

3.3.3 Detailed Spatial Variability

Here we present 2 snapshots of daily SST values, in order to compare more detailed GETM results with satellite derived temperatures. The sea surface temperature simulated with GETM-QU and the respective satellite data for July 05 are shown in figure 13.

The reason for selecting 5 July, 1989 was that this was the only rather cloudless day during all the summer months 1989, such that a nearly complete night time satellite SST image was available for comparison. The second best coverage, but having at the same time stronger horizontal gradients was obtained at 20 August, 1989. The model results and the satellite SST's are displayed in figure 14. Still not even the whole Common Area is cloud-free unfortunately, especially the area near to the German coast is not covered in the image from August. The general appearance of decreasing temperatures from about up to 18 ^oC in the Southern North Sea down to about 13 ^oC at about 57 ^oN is seen in the satellite SST and in the model data. The horizontal gradient in the satellite SST is smaller than in the model data.

The model shows up-welling in the Skagerrak area, which seems not to be present in the satellite's SST. These cold temperatures indicating up-welling in the Skagerrak and the Norwegian Trench seems to be a quasi permanent feature and must be investigated in more detail. Clearly, as only 2 single snapshots for comparison are available, we cannot expect detailed coincidence of the two SST data sets.

3.3.4 Discussion

The internal Rossby radius in the North Sea ranges from about $\sim$ 3 km in river plumes to about $\sim$ 20 km in the Norwegian Trench. Therefore the used model setup could not resolve details of the baroclinic features in the North Sea.

The occurrence of river plumes, confined to the coasts, can be seen in the respective plots of sea surface temperature. How much they are trapped to the coast is dependent mainly on the tracer advection scheme used. Lower order schemes, which are more diffusive, reduce horizontal gradients considerably.

The simulated annual cycle of SST in the North Sea agrees rather well with the satellite data. The specific choice of an uppermost layer, which is at almost constant depth below the surface, helps to compare the model results to satellite data. This represents a clear advantage compared to the use of traditional σ coordinates.

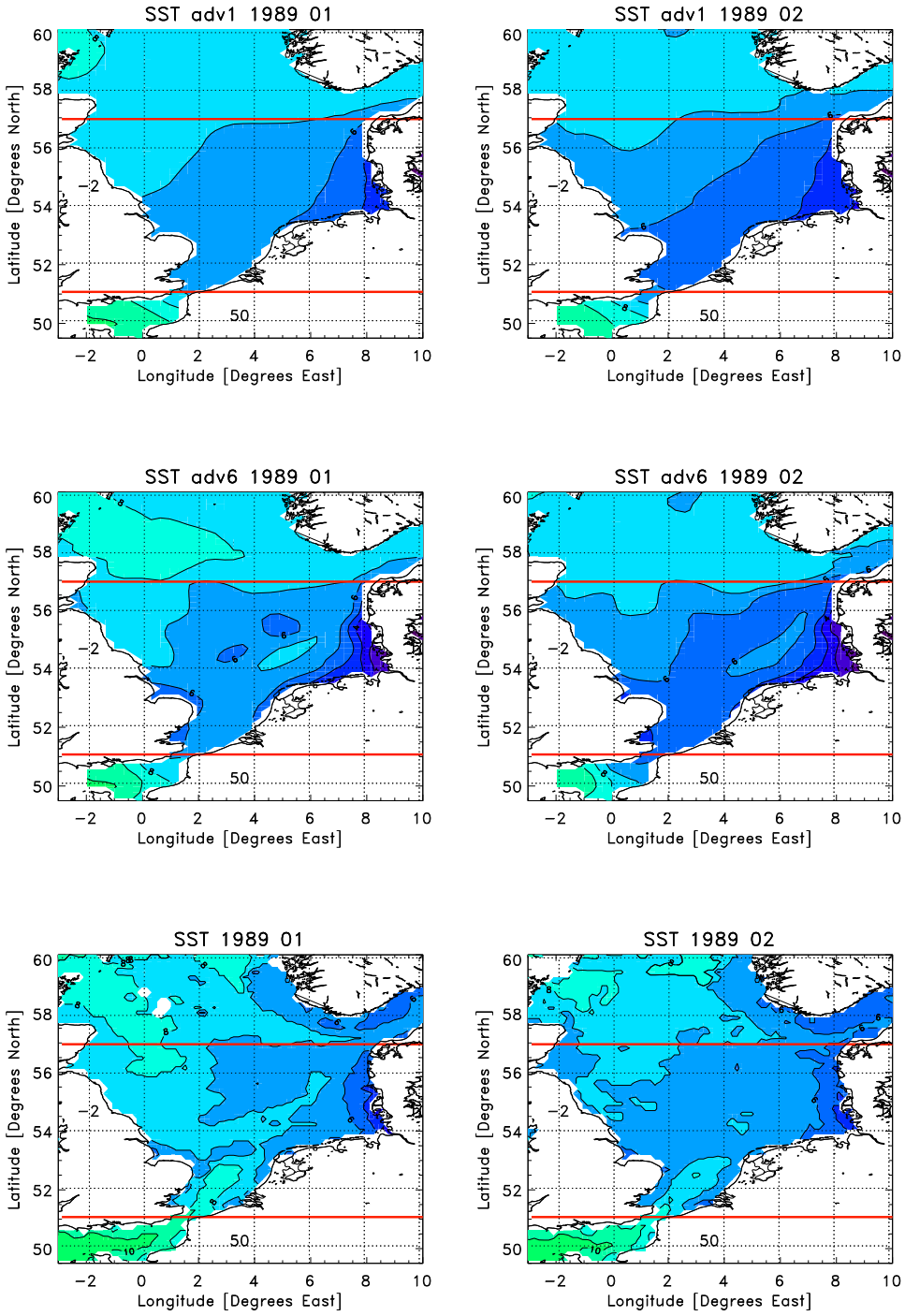

Fig. 11. Monthly mean SST from GETM-UP (upper panel), GETM-QU (middle panel) and NOAA Pathfinder satellite (lower panel) for the months January and February 1989.

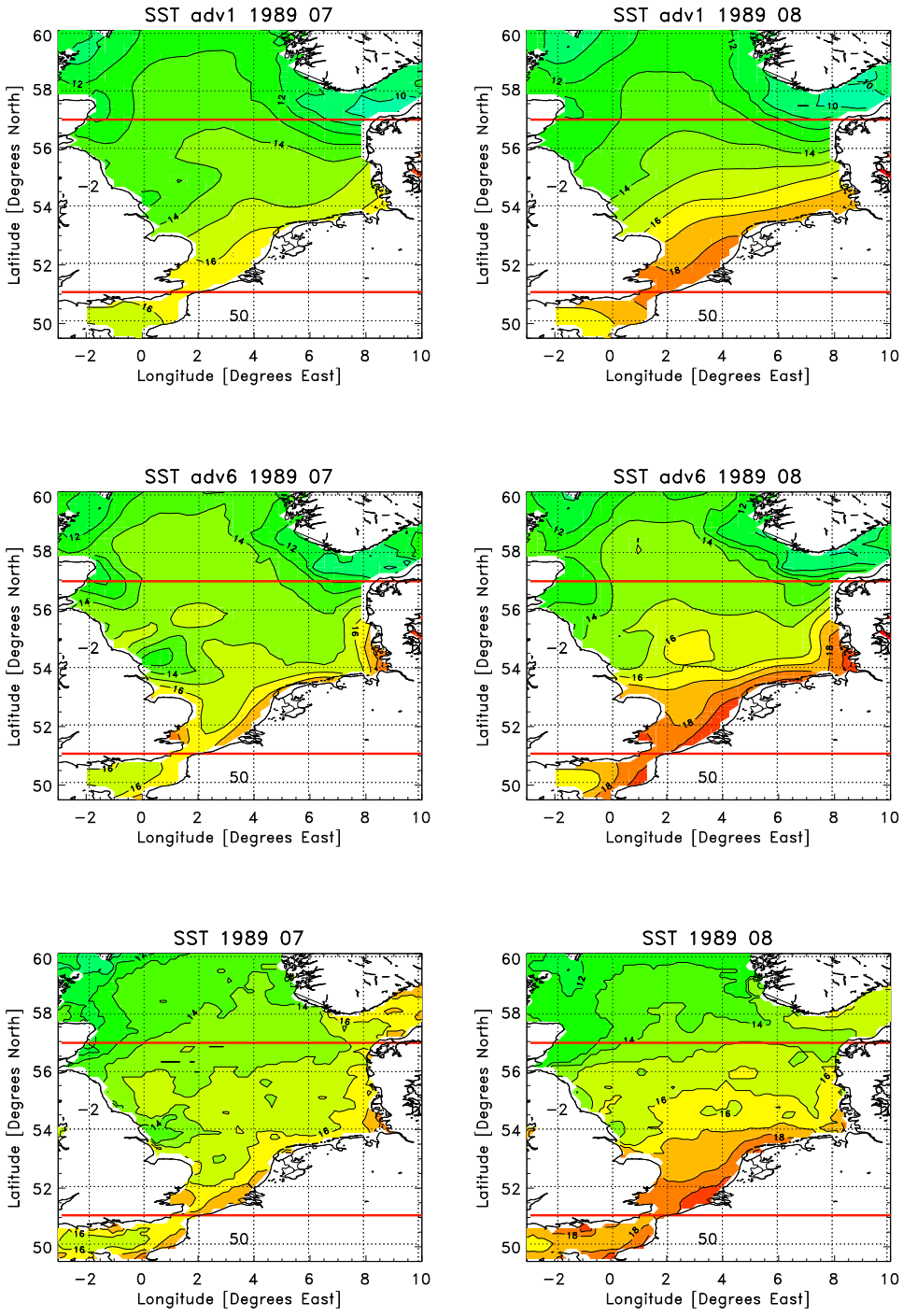

Fig. 12. Monthly mean SST from GETM-UP (upper panel), GETM-QU (middle panel) and NOAA Pathfinder satellite (lower panel) for the months July and August 1989.

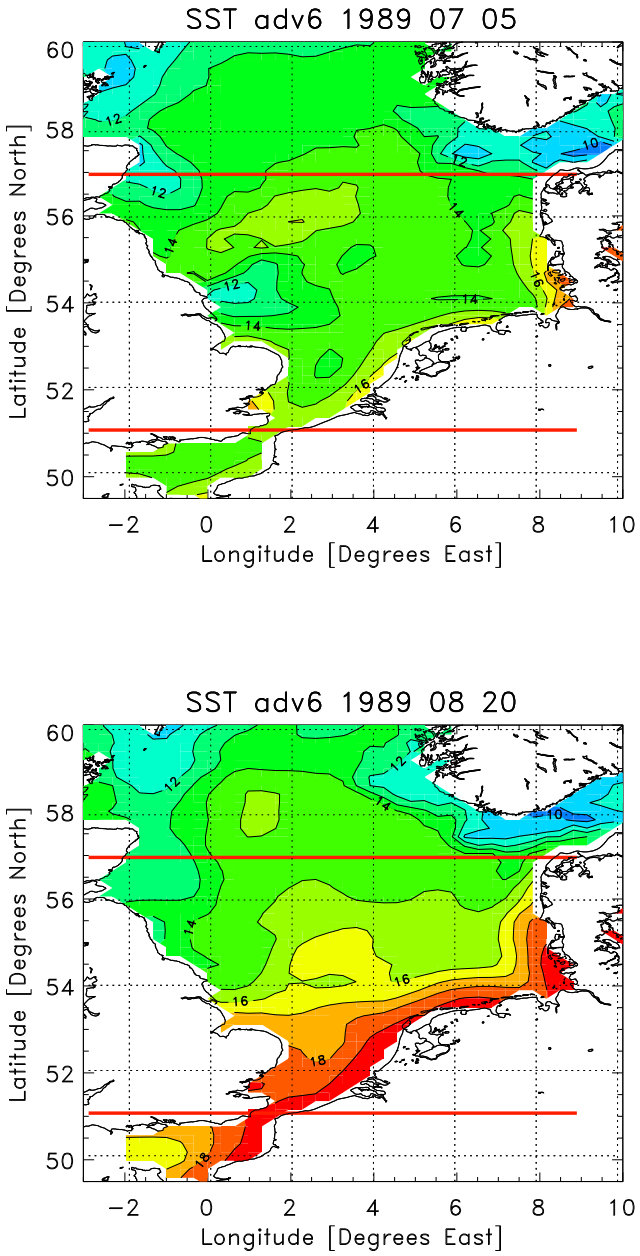

Fig. 13. Sea surface temperature simulated by GETM using QUICKEST tracer advection at 05 July, 1989 (upper panel) and the corresponding satellite data (lower panel, day 186)).

The monthly mean values of simulated and satellite SST show principally the same features. The imposed initial temperature was below the satellite SST values, therefore in the winter months the simulated SST's are colder than the measured ones, but showing a similar structure. During the summer months the agreement is improved and especially the results from the GETM-QU run

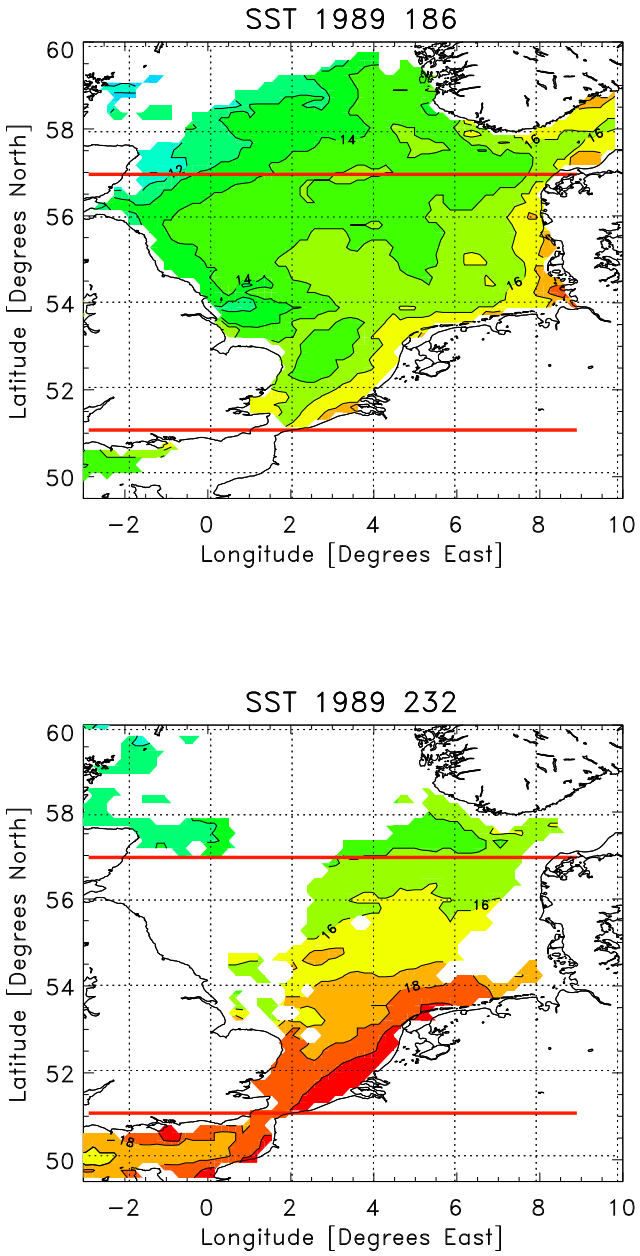

Fig. 14. Sea surface temperature simulated by GETM using QUICKEST tracer advection, 20 August, 1989 (upper panel), and the corresponding satellite data (lower panel, day 232). Same colours were used as in figure 13.

give some confidence in the simulations.

We undertook some effort to compare daily satellite SST's to model results. Unfortunately we must acknowledge that this is practically not feasible, because of the northern location of the North Sea, there are too many days

obscured by clouds. Therefore it seems necessary to rely in such comparisons on at least 8 daily or monthly SST averages. The disadvantage of this approach is clearly, that any synoptic variability which is in the order of 3-4 days in that area will be filtered out. To test the short term response of such 3D models against satellite SST's, will therefore not be that easy in such northern areas.

4 General model setup for coarse and fine resolution runs

4.1 Bathymetry

For the multi annual simulations a coarse resolution 6 nm × 6 nm and a fine resolution 3 nm × 3 nm cartesian model grid, were used.

These simulation are based on Cartesian grids, which have been extracted from the 1 nm × 1 nm DYNOCS bathymetry, see Weiergang and Jønsson (1996). The Baltic Sea data have been compiled by Seifert and Kayser (1995)

These grids have been generated by means of averaging the high-resolution 1 nm × 1 nm DYNOCS grid to the coarser grids by taking the maximum depth of the 1 nm × 1 nm grid boxes inside the coarse grid box as local value for the coarser grid. For the 6 nm × 6 nm grids only the central 4 × 4 1 nm grid boxes have been considered for the grid generation. For both grids, the grid boxes were set to land, when more than 50 % of the original 1 nm × 1 nm grid boxes were land points. This has consequences for the narrow Danish straits, e.g. the Little Belt and for the Øresund, which were closed by this procedure. Reopening the Little Belt by hand and using the original depth from the high resolution data resulted in an unrealistic high cross -sectional area and consequently to a far too high volume transport trough the Little Belt. Therefore the the Little Belt had to remain closed for the realistic simulations. Because of the importance of the Øresund for the salinity flux from Kattegat to the Baltic Sea, it had to be opened by hand. As the cross-sectional area is larger then in reality, volume and salt fluxes trough the Øresund are overestimated in the current model simulations. This original derived 3 nm cartesian model grid is presented in figure 15.

Several simulations were done using this bathymetry. This rather rough bathymetry creates problems for models using terrain following co-ordinates, as there are significant areas in which the hydrostatic consistency criterium is violated and additional artificial vertical mixing is created. Therefore an iterative selective smoothing 9-point filter has been applied. The criterium for selecting specific points to be smoothed, is based on the search for R_{values} (an expression for the steepness of the bathymetry), which exceed 0.4. The R_{value} is defined by

$$R_{value} = \frac{max(\partial_x H, \partial_y H)}{H} < 0.4 \tag{19}$$

Therefore a steep slope in shallow parts is more dangerous than in deeper parts of the Sea. Typically about 10 iterations were done, but this procedure does normally not converge, so that some points (in the order of 200) will still have R_{values} exceeding 0.4 after this procedure.

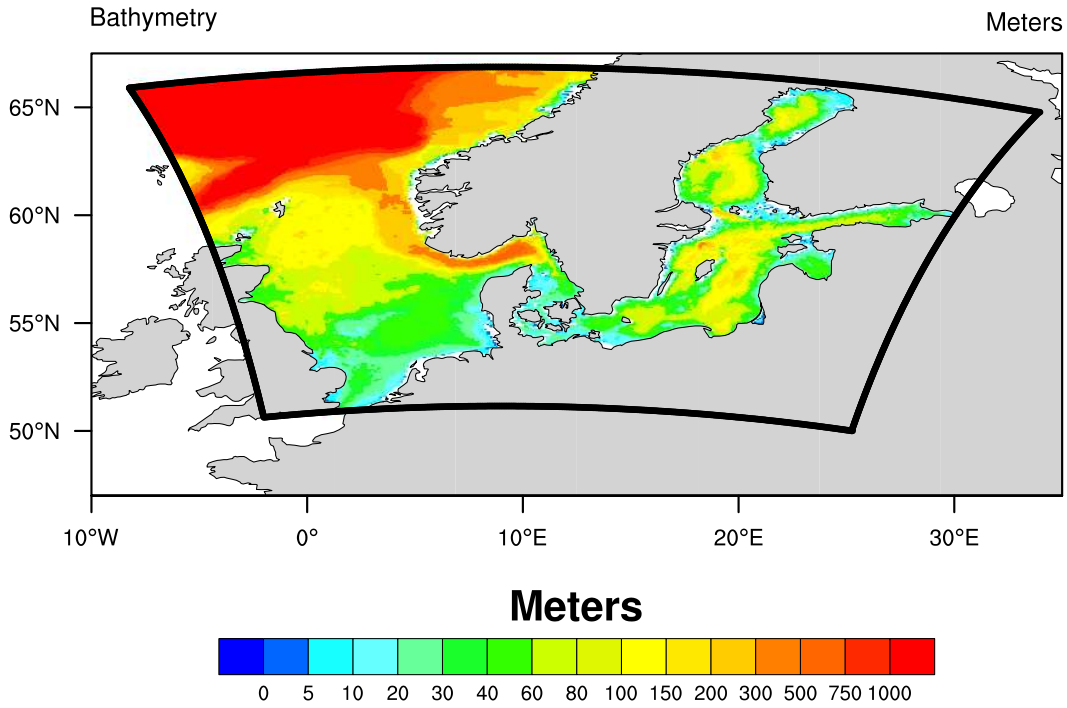

Fig. 15. Un-smoothed bathymetric chart of the North Sea and Baltic Sea, used for the 3 nm fine resolution simulations.

Different time steps had to be used in order to account for the CFL criterium for long barotropic waves. The time step for the coarse resolution simulation is $dt = 45\ s$ and for the fine resolution it is $dt = 22.5\ s$.

4.2 Meteorological data

The major data set used in this study for investigating the meteorological conditions and as well for forcing the 3D hydrodynamical model are meteorological parameters provided by the European Centre for Medium Range Weather Forecasting (ECMWF, www.ecmwf.int). The following basic parameters were extracted from the ECMWF data base: air pressure, air temperature, total cloud cover, wind speed (east and north component) and dew point temperature. The time step of the data is 6 hours and the spatial resolution is 0.5 degrees. The data are spatially interpolated to the respective model grid.

For calculating the air-sea exchange fluxes bulk parameterisations (Kondo (1975)) using the above data and the model sea surface temperature (SST) were applied. Finally the fluxes are interpolated to each micro time step. During 2004 also a parameterisation for precipitation and evaporation/condensation was implemented.

4.3 Initial conditions

For the initial conditions the climatological data set compiled by Janssen et al. (1999) for the Baltic Sea and the North Sea has been used. For this data set, more than 3.1 million temperature data and 2.9 million salinity data points have been interpolated to a 10 km $\times$ 10 km grid containing monthly mean values distributed over 18 vertical layers. In order to use these data for the present simulations, they are horizontally (linearly) interpolated to the model grid by taking into account 4 climatology grid points around a model grid point. In case one or more of these climatological data points are on land and thus not associated with physically correct values, they are set to values of adjacent grid points first. Such horizontally interpolated files are then read into the model, where they are vertically (linearly) interpolated to the actual model grid.

Since the baroclinic model runs are generally initialised on December 15, 1986 and run in diagnostic mode for the first two weeks, the model temperature and salinity are initialised with the climatological values for December, which are here understood as representative for December 15.

4.4 River inflow

Climatological riverine freshwater inflow from the following 30 generalised rivers, provided by Thomas Neumann from the Institute for Baltic Sea Re-

search is considered in the simulations presented here:

1. "Elbe"	2. "Ems"	3. "Forth"
4. "Tees"	5. "Humber"	6. "Somme"
7. "Seine"	8. "Rhine/Meuse"	9. "Tyne"
10. "Scheldt"	11. "Thames"	12. "Wash"
13. "East Norway 1"	14. "East Norway 2"	15. "East Norway 3"
16. "East Norway 4"	17. "Oder"	18. "Weichsel"
19. "Njemen"	20. "Daugawa"	21. "Narva"
22. "Neva"	23. "Kokemaki"	24. "Kemijoki"
25. "Lulealv"	26. "Umealv"	27. "Angermansalv"
28. "Maelaren"	29. "Eman-Motal"	30. "Helegan"
31. "Goetaalv"	32. "Baie St. Michel"	33. "Ijsselmeer"

The temperature of the fresh water inflow was assumed to be the ambient temperature. The geographical positions at which this freshwater is supplied to the model domain are shown in figure 16.

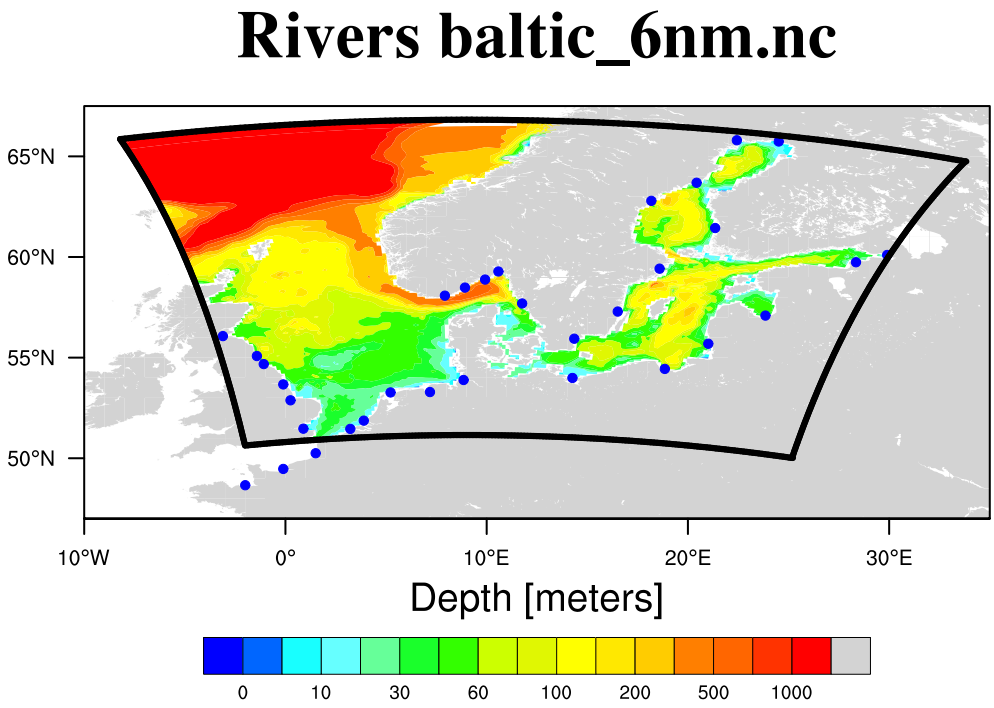

Fig. 16. Map of the North Sea and the Baltic Sea showing the riverine freshwater run-off positions for the 32 rivers considered for the present simulations.

4.5 Tidal forcing

For the tidal forcing at the open boundaries towards the Norwegian Sea and the English Channel, the TOPEX-POSEIDON data set had been used, see `http://podaac.jpl.nasa.gov/cdrom/tide/index.html`. In total, 13 partial tides have been considered. The data have been extracted from the TOPEX-POSEIDON data set and interpolated linearly in time and space to the open boundary elevation points. The time frequency of the tidal data is hourly.

4.6 Open boundaries

For constructing the 3D open boundary conditions, again the climatological data set compiled by Janssen et al. (1999) for the Baltic Sea and the North Sea has been used.

To use this data for the present simulations, they are first horizontally (linearly) interpolated to the boundary grid points by taking into account 4 climatology grid points around a boundary grid point. Such horizontally interpolated files are then read into the model, where they are vertically (linearly) interpolated to the actual model grid. The monthly climatological boundary data are then linearly interpolated to the actual model time.

4.7 Implementation details

For the spatial discretisation a staggered C-grid is used. GETM allows the selection of different order scalar advection schemes, as e.g. UPSTREAM (UP) and the ULTIMATE QUICKEST (QU) scheme, which were used here for comparison and sensitivity studies. The advection schemes can be applied to transport temperature and salinity and separately also momentum can be treated with a higher order scheme, for details see Burchard and Bolding (2002). Tested was also the Flux Corrected Transport (FCT) advection scheme by Zalezak (1979), which advects the two horizontal directions in one step. For this application the results were not significantly improved. Therefore we have chosen to generate the final results with the ULTIMATE QUICKEST scheme to advect momentum, temperature and salinity.

The vertical discretisation is done using general vertical coordinates, which interpolates between equidistant and non-equidistant σ-transformations. For the runs done in 2002 and 2003 the critical depth is set to 40 m and the grid is refined to surface (ddu=2) and bottom (ddl=1). To give an impression of the layer distribution obtained by using such transformations, figure 17 shows

the layer distribution along a zonal section at about 58^o N from the North Sea, via Skagerrak, Sweden and the Baltic Sea. A meridional section trough the Baltic Sea at about 16^o E is presented in figure 18. The final runs done during 2004 avoided the refinement towards the bottom (ddl=0) and instead a strong refinement to the surface (ddu=5) was used.

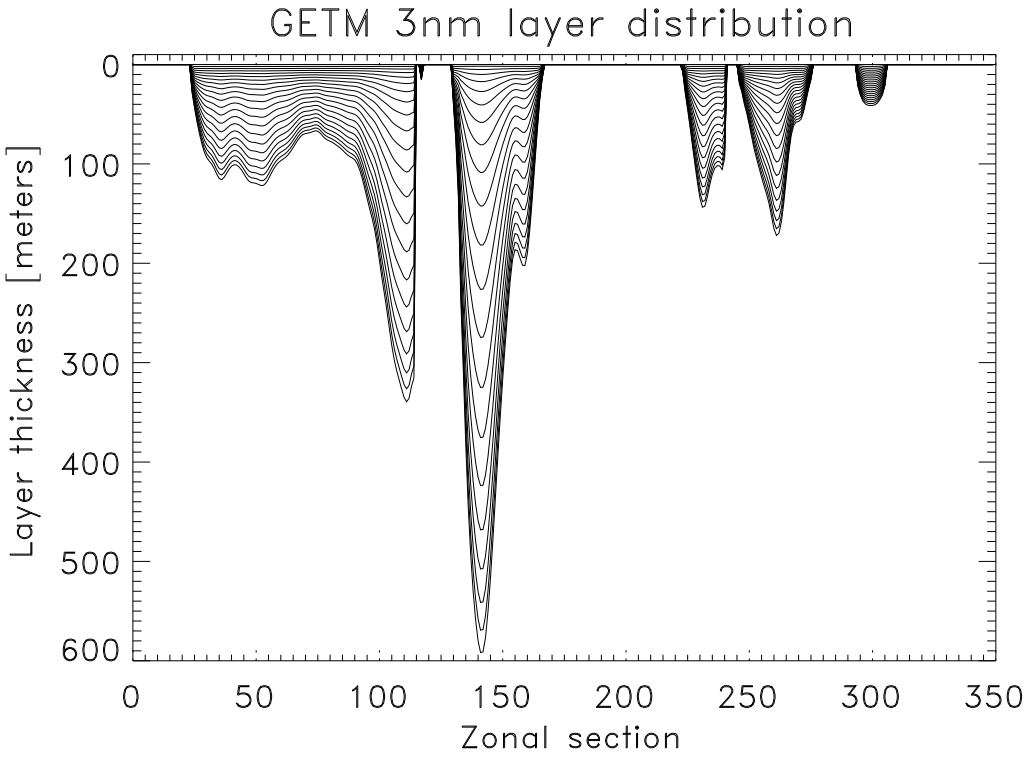

Fig. 17. The plot shows the vertical layer distribution for a zonal cross section at about 58^o N, as used for the present fine resolution simulations.

The turbulence scheme of GETM is chosen via the GOTM turbulence model. In this study we used the standard k-ε turbulence closure, without imposing a length limitation or background vertical diffusivity. GETM uses different time steps for the internal (macro time steps) and the external mode (micro time steps). For all simulations presented here, a bottom roughness length of $z_0^b = 0.01$ m has been used. The chosen micro time step for the coarse/fine setup is 45 s/22.5 s, the split factor is 30, which gives in this case a macro time step of 1350 s/675 s.

To parameterise the light attenuation in such a large area having rather large variations in turbidity a compromise had to be made. According to the Jerlov (1968) classification (see figure 72 there) the North Sea would belong to ocean water type III, whereas the Baltic Sea would belong to coastal water type 3. We used the mean value for the percentage of total irradiation between these

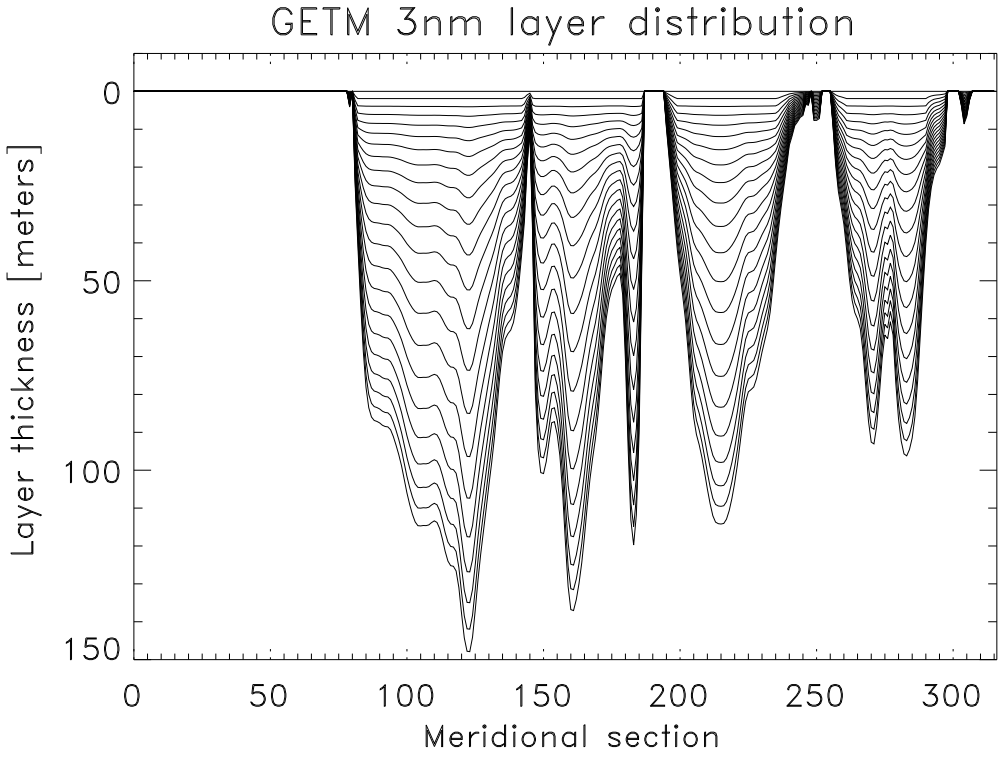

Fig. 18. The plot shows the vertical layer distribution for a meridional cross section at about 16^o E (Baltic Sea), as used for the present fine resolution simulations.

two types and calculated new attenuation coefficients. A further motivation for the recalculation of attenuation lengths is, that Stips et al. (2002) have shown that parameterisations of attenuation lenghts following Paulson and Simpson (1977) are not good in the uppermost meter (calculated irradiance is higher than that for pure water). The newly calculated and used attenuation lengths are $a = 0.57$, $l_1 = 0.34$ m, $l_2 = 5.5$ m, with $\eta_1 = 1/l_1$ see section 2.

The imposed boundary conditions for temperature and salinity are relaxed to the model values using a 5 point sponge layer. To better resolve the shallow parts of the North Sea we decided to use general vertical coordinates with a slight zooming towards the surface and the bottom. The surface layer thickness has been chosen to be two metres overall.

In order to investigate the influence of the horizontal momentum diffusion, different values for the background horizontal diffusion were applied, reaching from very low diffusion coefficients of $A_M = 0m^2s^{-1}$ or $A_M = 10m^2s^{-1}$ over a medium high diffusion of $A_M = 100m^2s^{-1}$ to a rather high diffusion of $A_M = 1000m^2s^{-1}$.

During 2002 and 2003 typically, all performed runs were done on one single

processor, using about 12 h to 16 h per simulated month for the fine grid. Therefore the multi-annual simulations took up to 2 to 3 months to finish. Since 2004 the model is running stable in parallel mode, typically on 9 processors for the fine resolution grid and hereby allowing more sensitivity studies and evaluation of different parameterisations.

5 Results of coarse and fine resolution simulations for the coupled North Sea - Baltic Sea model

5.1 Sea level at selected stations

The correct reproduction of the water elevation is the most basic requirement for 2D/3D hydrodynamic models, as this determines the quality of the simulations. All tidal simulations discussed here are only forced by astronomical tidal elevations from the TOPEX-POSEIDON data set, see section 4.5. This forcing is applied at the northern open boundary of the North Sea and the southern open boundary at the British Channel, which means far away from our region of interest in the Baltic Sea. The measured and simulated sea level at the tidal gauge Warnemünde are shown in figure 19, for the two years 1992 and 1993. Many features are well reproduced by the simulations, as e.g. the quick sea level change in January 1993, which resulted also in a corresponding salt water inflow. The linear correlation coefficient between measured and simulated sea level is 0.7. Anyhow certain periods show larger and unsatisfactory deviations as e.g. during April and May 1993. The sea level in this area is mainly determined by the large scale atmospheric pressure fields and at shorter time scales also by the prevailing wind directions. Using improved ECMWF re-analysis data (ERA40) led to improvements in the sea level simulations. It could be expected that for the fine resolution grid the agreement between model results and station data would be better, because of the better approximation of the bathymetry. Contrary to this expectation, for the water elevation at Warnemünde this is not the case (figure 19).

The sea level at Landsort is considered as representative for the Baltic Sea. Further to this, Gustafsson and Andersson (2001) demonstrated that the air pressure difference between Oksoy (Norway) and de Bilt (Netherlands) is very well correlated to the water elevation at Landsort and therefore this pressure difference is a good indicator for salt water inflows into the Baltic Sea. We tested this using the air pressure difference derived from the ECMWF analysis data and sea level at Landsort from the coarse resolution run. Both data sets are plotted in figure 20 and the suggested good correlation between them can be confirmed. Therefore the quality of ECMWF forcing data is sufficient to reproduce qualitatively salt water inflows into the Baltic Sea.

Finally, detailed astronomical tidal prediction data are compared to model results for a tidal gauge station at Grenaa (Denmark, Kattegat), figure 21. The tidal predictions were calculated from a harmonic analysis of tidal gauge data and provided by the Royal Danish Administration of Navigation and Hydrography (Farvandsvæsenet). The considered time interval is March 2001, where the first two weeks are shown. Both selected resolutions show good

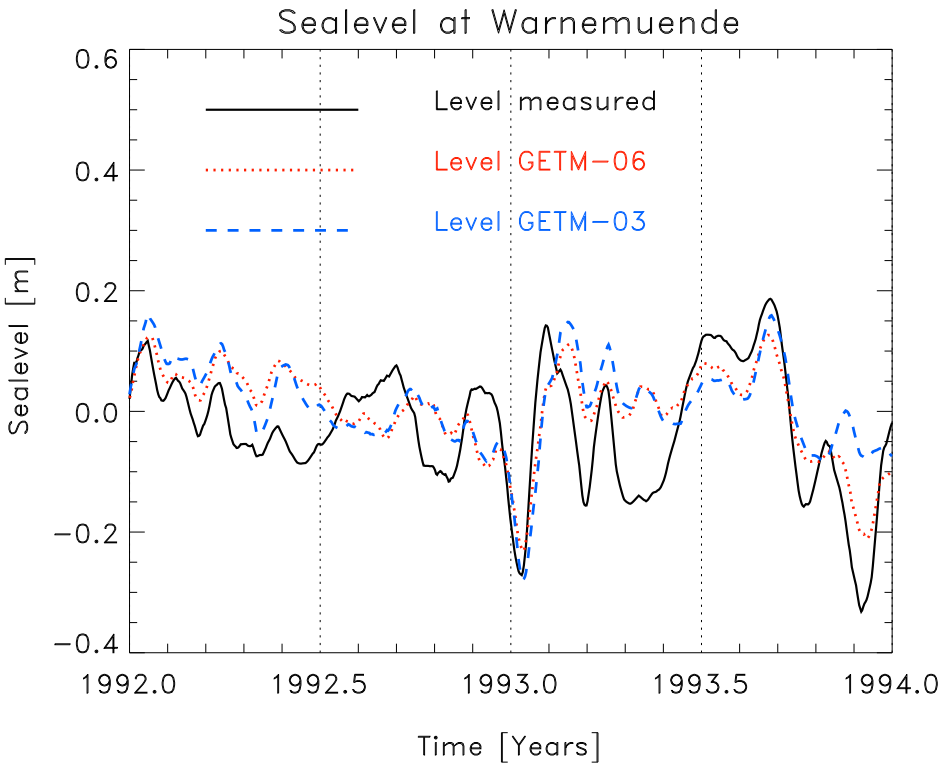

Fig. 19. Comparison of measured and simulated sea level at tide gauge Warnemünde (Germany).

agreement with the tidal predictions, but surprisingly in this case even the coarse resolution model gives better results than the fine resolution model. This was not the case for all the other investigated tide stations. In general it can be concluded that the reproduction of astronomical tides is increasingly difficult with more complex bathymetry. Therefore a good and realistic representation of the underlying bathymetry is a precondition for achieving high quality model results.

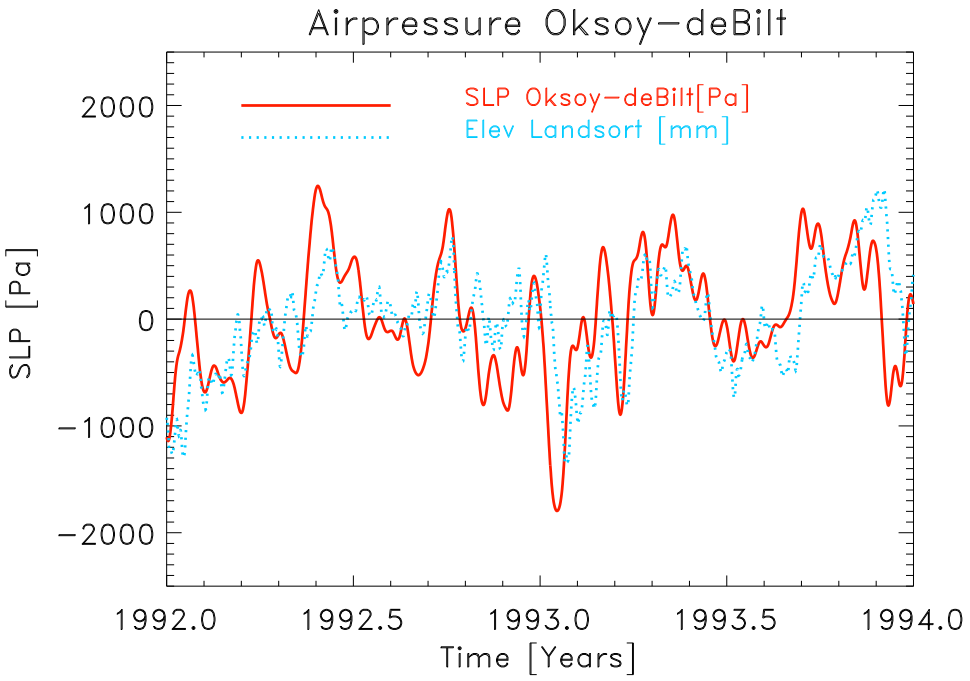

Fig. 20. Comparison between simulated sea level (multiplied by 4000 in order to scale approximately with the pressure data) at Landsort and air pressure difference between Oksoy and de Bilt derived from ECMWF data.

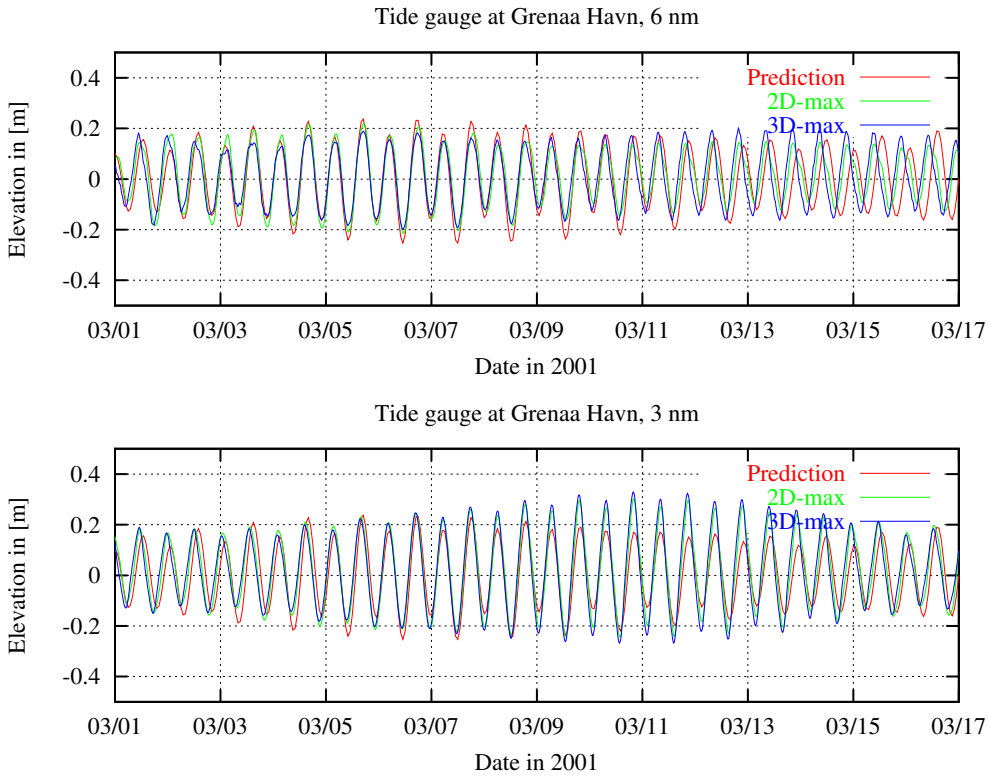

Fig. 21. Predicted and simulated tidal elevations for GrenåHavn for the 6 nm grid (upper panel) showing the 2d and 3d results and the 3 nm grid (lower panel).

As the oxygen conditions in the deeper basins of the Baltic Sea are critically dependent on the salt exchange between the North Sea and the Baltic Sea, since many years great research efforts have been undertaken to understand and to simulate or even forecast the respective inflow events.

A contour plot of salinity over depth and time at the station Darss Sill for 1992 and 1993 is presented in figure 22. The signature of the major salt water inflow during January 1993 (Matthäus and Lass (1995)) covering the complete water column can be clearly identified. The simulated maximum salinity of the in flowing water (15 PSU) is smaller than the observed maximum of about 20 PSU. In the lower panel model results from the final 2004 rerun are shown. First it is obvious that the vertical stratification is now much stronger, which is in better agreement with reality. Second, also the maximum salinity at the bottom is now about 19 PSU, which is closer to those measured.

In figure 23, simulated surface and bottom salinities at the Darss Sill are compared to measured data from the monitoring programme of the institute for Baltic Sea Research. Unfortunately for that time only some single snapshot measurements are available. Anyhow a general agreement between simulated and measured data can be found. Typically we find at the Darss Sill a pronounced salinity stratification, due to inflowing saline bottom water and outflowing fresh surface water. This typical feature is disrupted by shorter periods of rather well mixed water column salinity. An especially long lasting mixed period occurs in spring 1992. The reduced vertical mixing and the therefore increased bottom salinity in the final runs from 2004 (new run) compared to the runs from 2003 (old run) is clearly visible.

After the Darss Sill the inflowing salt water enters the Arkona Basin before it can continue to the Bornholm Basin and finally enter the deep Gotland Basin. As the Arkona basin is about 40-45 m deep, the saline water will remain at the bottom, therefore the Arkona Basin will always remain salt stratified. This behaviour of the salt inflow during January 1993, can be seen in figure 24 (data from old run), which clearly shows that the more saline water is limited to water depths below 30 m.

Gustafsson and Andersson (2001) proposed that the Kattegat surface salinity can be reproduced by the Baltic Sea level (which is represented by the Landsort sea level), because of the linear relationship between the two. We wanted to test this hypothesis, by using the simulated Kattegat surface salinity and comparing it to a hypothetically derived salinity from the simulated Landsort sea level. The results of this exercise are presented in figure 25.

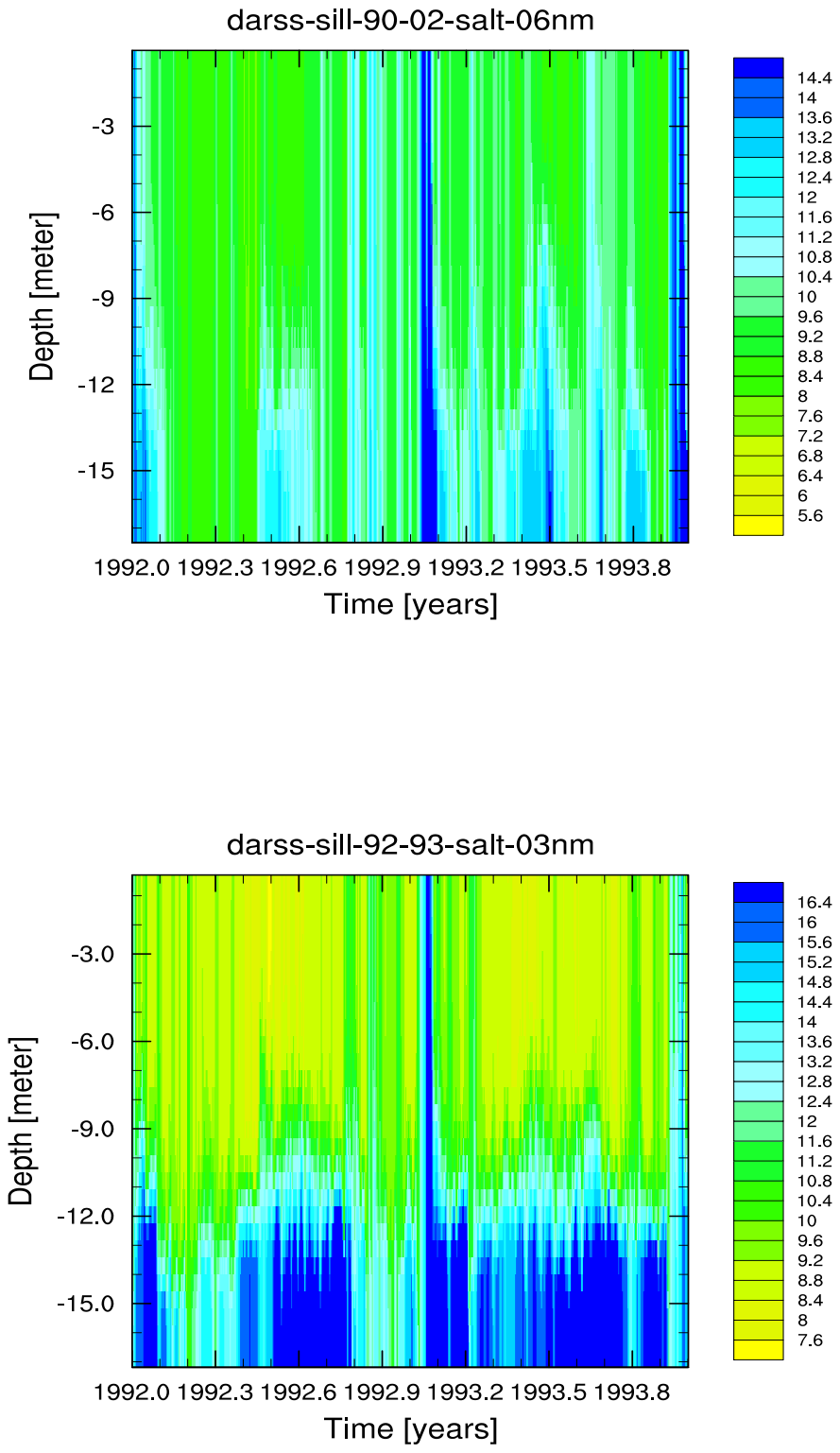

Fig. 22. Contour plot of salinity at the entrance to the Baltic Sea, the Darss Sill (upper panel shows simulation done in 2003). The signature of the major salt water inflow during January 1993 covering the complete water column can be identified by the blue colour. The lower panel shows the results from the 2004 final run.

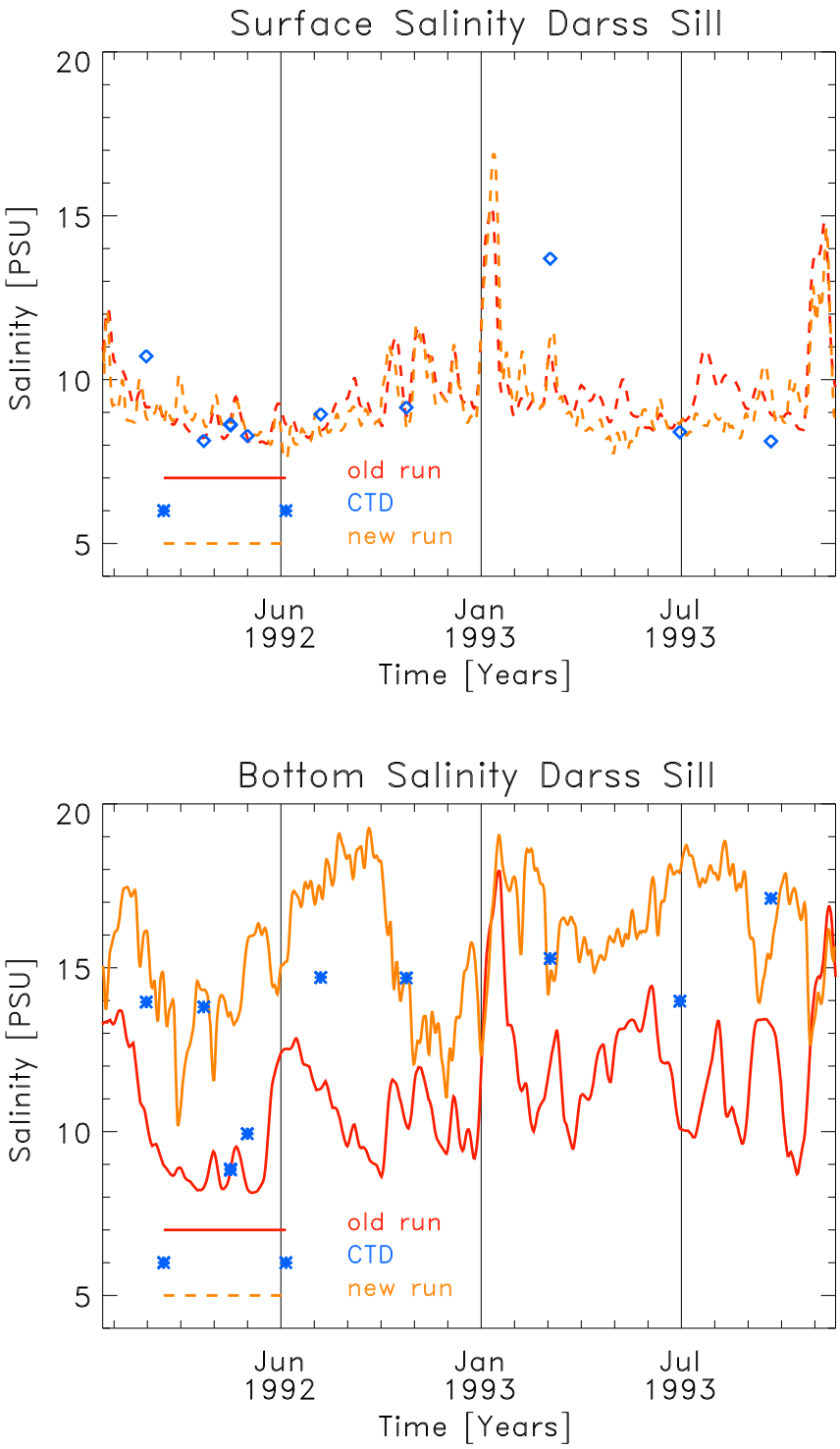

Fig. 23. Surface and bottom salinity at the monitoring station Darss Sill. Simulated salinities are presented by the line, whereas the measured data are indicated by symbols.

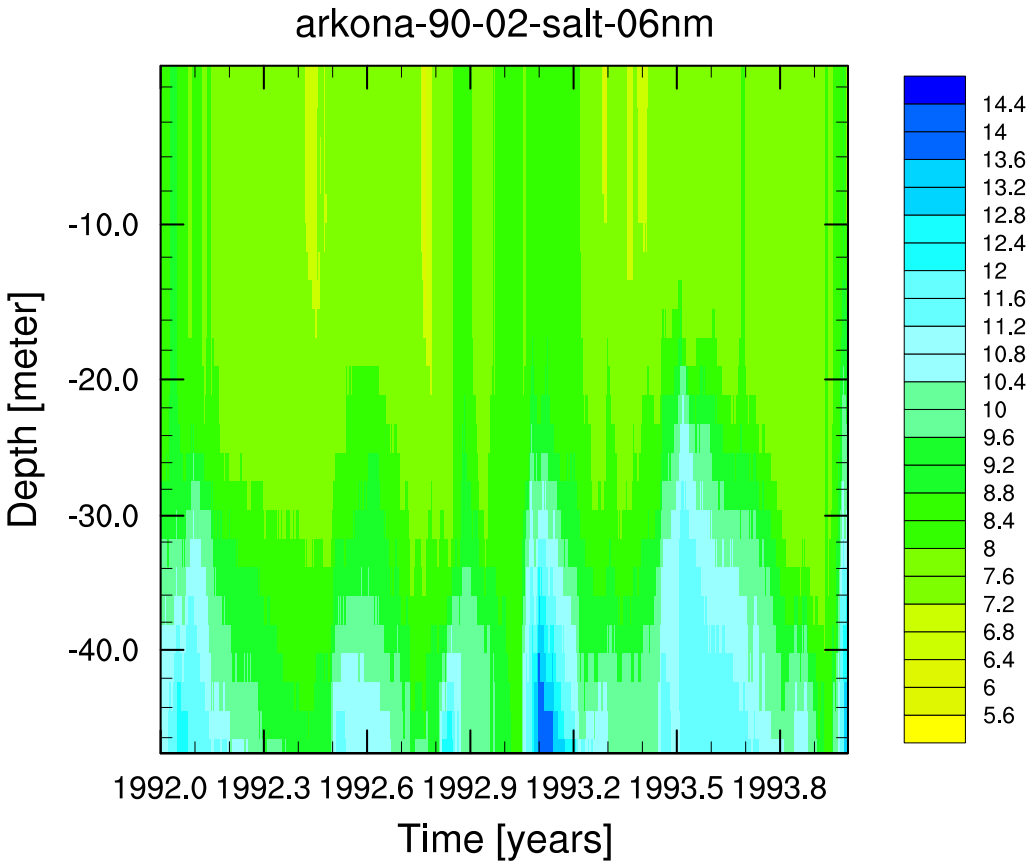

Fig. 24. Contour plot of salinity at the central station of the Arkona Basin. The signature of the major salt water inflow during January 1993 can be identified by the blue colour between 45-40 m depth.

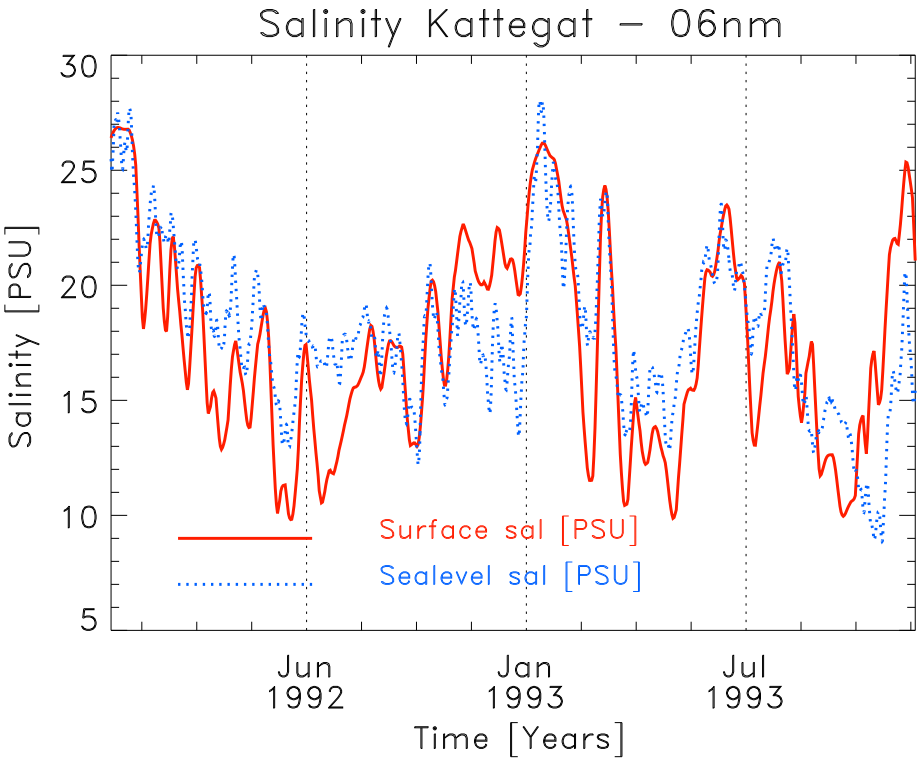

Fig. 25. Simulated surface salinity at Kattegat (red line) compared to surface salinity estimated from Landsort sea level (blue line). The rather good correlation between these two curves is obvious.

Reproducing salt water inflows with typical z-level models as the Modular Ocean Model (MOM) used at the Institute for Baltic Sea Research or HIROMB used at the Swedish Meteorological and Hydrological Institute (SMHI) is hampered by difficulties introduced by the discontinuous bottom topography, which results in enhanced mixing of the transported salt water. Therefore even strong salt water inflows do not arrive finally at the Gotland Basin, as the salt water tongue is already strongly diluted in the Bornholm Basin. Using terrain following co-ordinates as in GETM it could be hoped, that an improved simulation of the spreading of the salt water tongue, into the central parts of the Baltic Sea can be achieved. That this is indeed the case can be seen in figures 26 and 27, which provides an impression of the time evolvement of the inflowing salty water. This case is a very interesting example of summer salt water inflows which occur outside of the main season for salt water inflows (winter) and have until recently not attracted much attention. Feistel et al. (2004) were one of the first who described such an exceptional (and in this case also warm) salt water inflow, which occurred during August and September 2003. Such inflows, which transport oxygen into the deep parts of the Baltic Sea are very important, because they lead to an oxygenation of the stagnating bottom layers. Unfortunately we do not have sufficient monitoring data in order to check how realistic this salt inflow was simulated (as e.g. the absolute salinities seem to be about 1 PSU too low), but the only available data from the Bornholm Deep (figure 28), seem to support this hypothetical mini-inflow in summer 1986. If this could be proven, it would be the first inflow discovered by numerical simulations of the Baltic Sea.

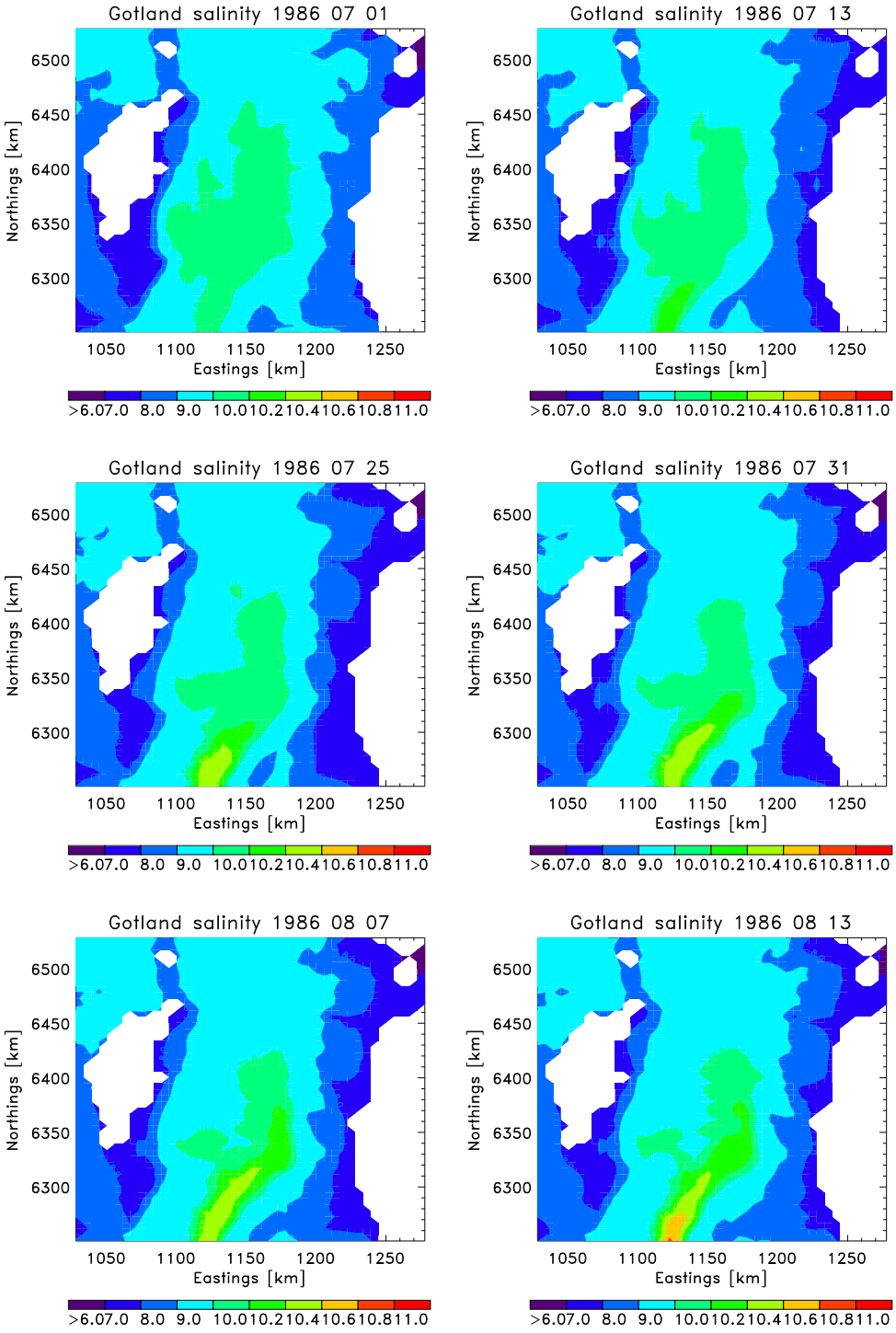

Fig. 26. Simulated bottom salinity in the central Gotland Basin (maximum depth 245 m), during July, August and September 1986. The spread of the in flowing salty water during this time can be clearly identified by the expanding bright colours of the salt tongue.

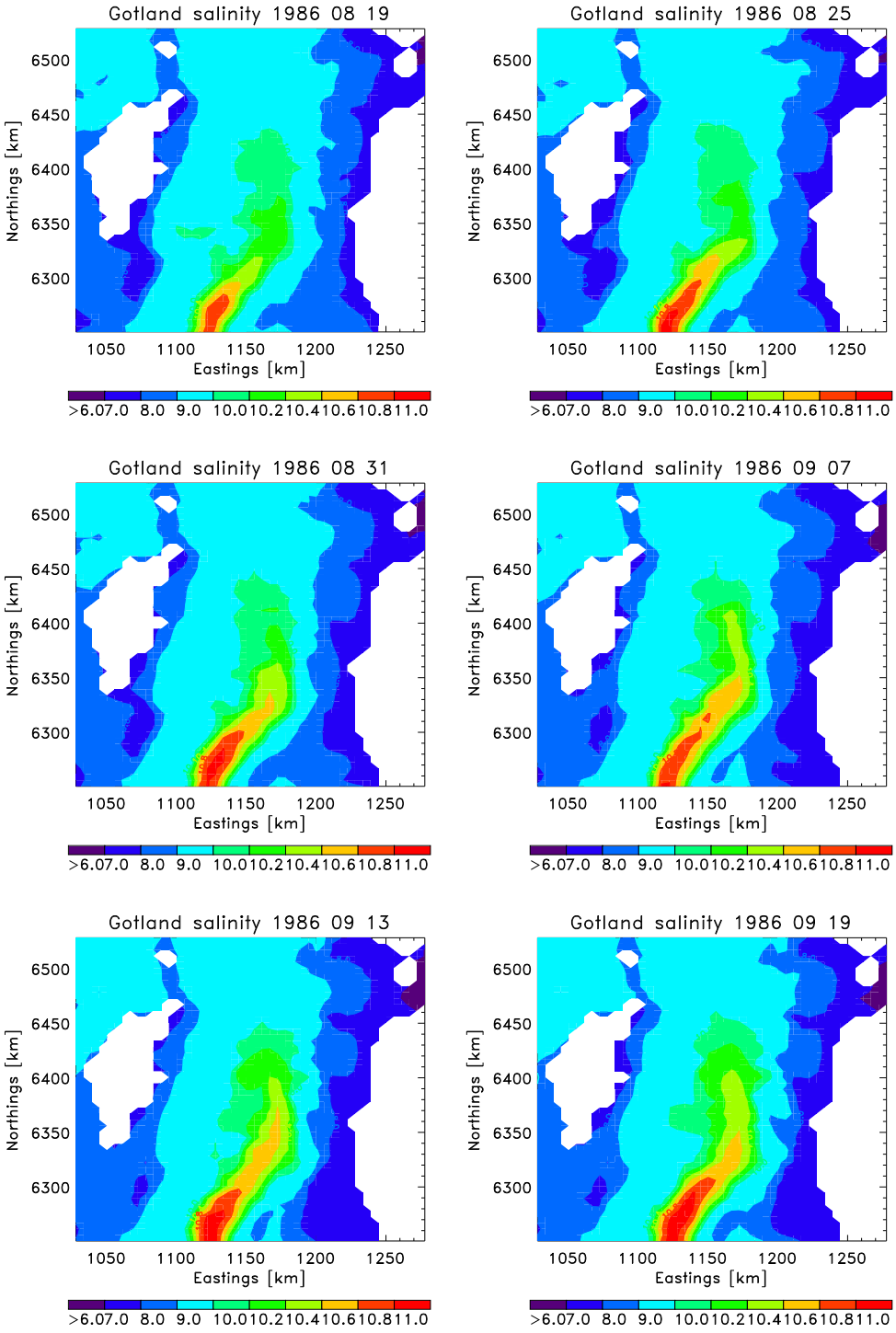

Fig. 27. Simulated bottom salinity in the central Gotland Basin (maximum depth 245 m), during August and September 1986. The spread of the in flowing salty water during this time can be clearly identified by the expanding bright colours of the salt tongue.

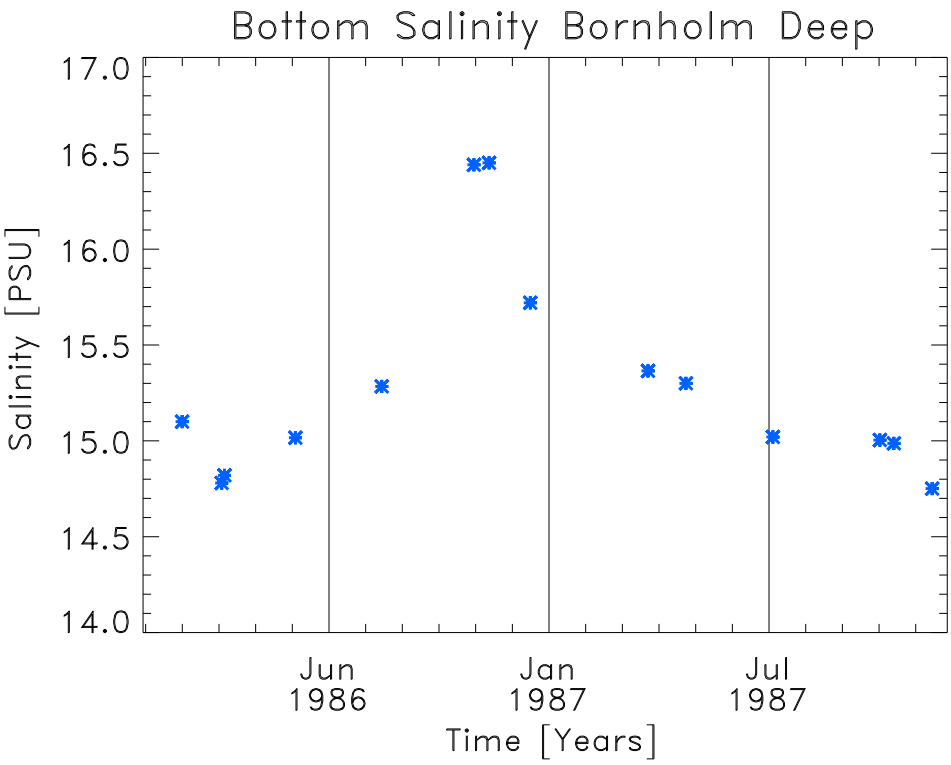

Fig. 28. Measured salinity at the Bornholm Deep during 1986 and 1987. Because of the sparse measurement frequency just during August and September 1986 data are missing, but the increased salinity in October indicates that saltier water was inflowing before.

5.4 Water flow trough the Danish Straits during 2002

5.4.1 Introduction

The horizontal water exchange involving the inflow of oxygen-rich bottom water from the Kattegat is critical for the development of oxygen deficiencies in the Belt Sea area. In order to investigate this and to compare our results to other simulations, water exchange through the Kattegat, Belt Sea and the Sound were calculated by two different 3D hydrodynamic models:

(1) The GETM model setup, as described above covers the North Sea and the Baltic Sea with a resolution of 3 nm and 25 depth levels in the entire area. For the investigated area, daily data and monthly mean values covering the period 1990-2002 were available.
(2) The Swedish Meteorological and Hydrological Institute (SMHI) operational model HIROMB (High Resolution Model of the Baltic) covers the Baltic Sea and the north-eastern North Sea with 3 nm resolution. HIROMB produces output of temperature, salinity, and current velocities at up to 16 depth levels. In the shallow water of the Belt Sea, four-hourly data covering the period 1998-2002, were available at 4, 8, 12, 18 and 24 metres.

Both models have therefore suitable characteristics for calculating flows in the Belt Sea area. Data from the HIROMB model were provided by Philipp Axe from SMHI. Output from the JRC model GETM was compared with that from the SMHI HIROMB model for validation purposes and to show the depth-integrated picture of exchanges through these seas. The SMHI and JRC models allowed to examine the contributions from different levels in detail.

To investigate the impact of horizontal water exchange involving the inflow of oxygen-rich bottom water of the Kattegat on the oxygen deficiency in the Belt Sea area, HIROMB accumulated flow from the 18-24 metre layer was calculated. For the same purposes, the absolute flow of the bottom layer (this is defined as the layer between the maximum density stratification and the sea bed) and the surface layer as derived from GETM was investigated, based on monthly mean values.

A more detailed view of the transition area between North Sea and Baltic Sea is given in figure 29.

5.4.2 Flow characteristics

Figure 30 presents the accumulated flow F_{acc} derived from GETM for the upper layer, the bottom layer and the entire water column for the Kattegat,

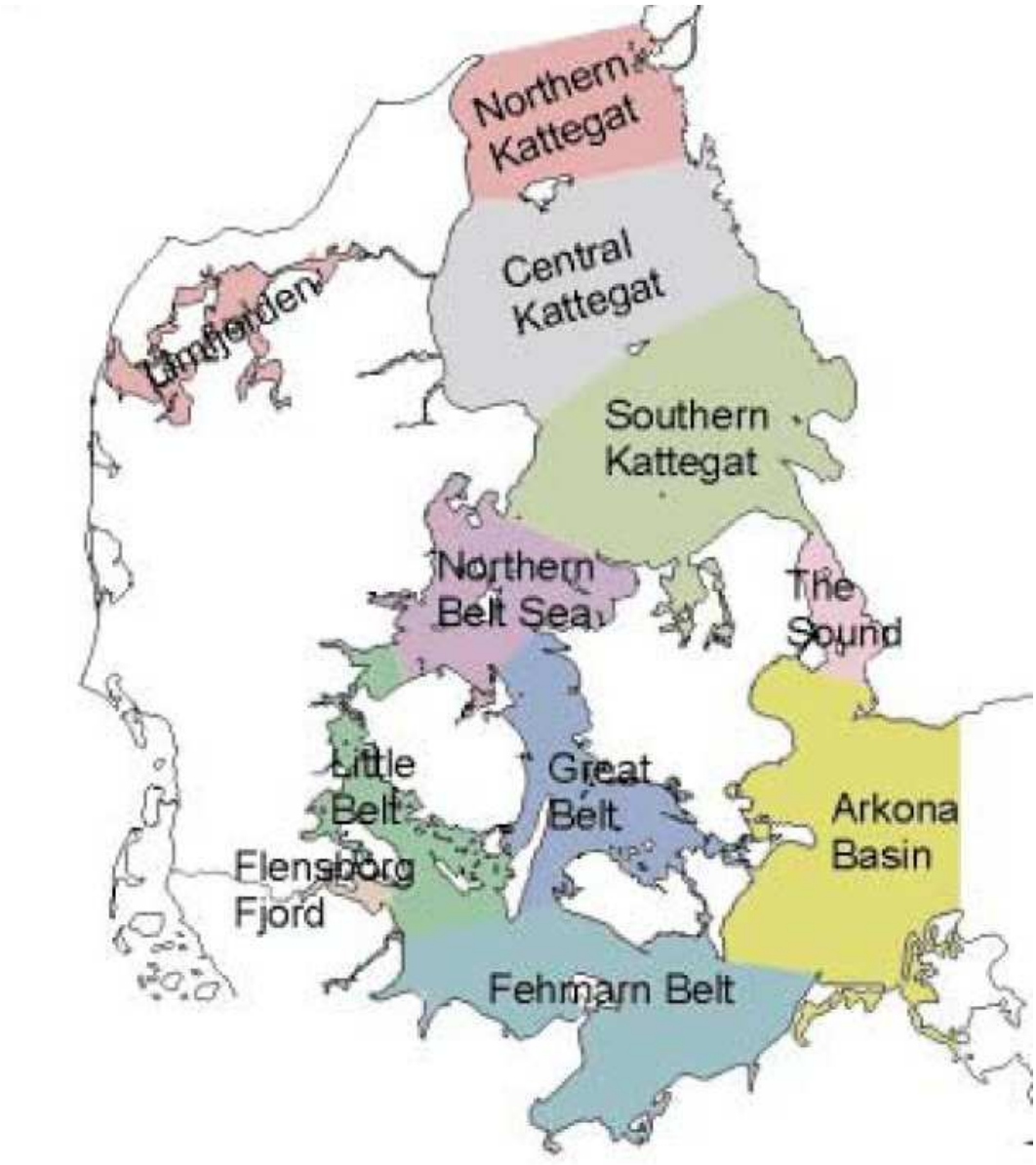

Fig. 29. Transition area between North sea and Baltic Sea, with respective name of the specific regions discussed in this report.

Gniben (comprising Great Belt and Little Belt) and Nyborg (only Great Belt) sections during 2002. The temporal flow variations and the total accumulated flow trough the Gniben section can be compared to the HIROMB output.

Figure 31 shows outflow through the Hasenøre-Gniben section (the border between the Kattegat and the Belt Sea) for the same period, calculated by HIROMB, for each depth layer (0-4 m, 4-8 m, 8-12 m, 12-18 m and 18-24 m), as well as the total outflow volume.

The two models agree reasonably, especially for the major flow variations. Differences may be due to the disparity in the forcing data, e.g. the water

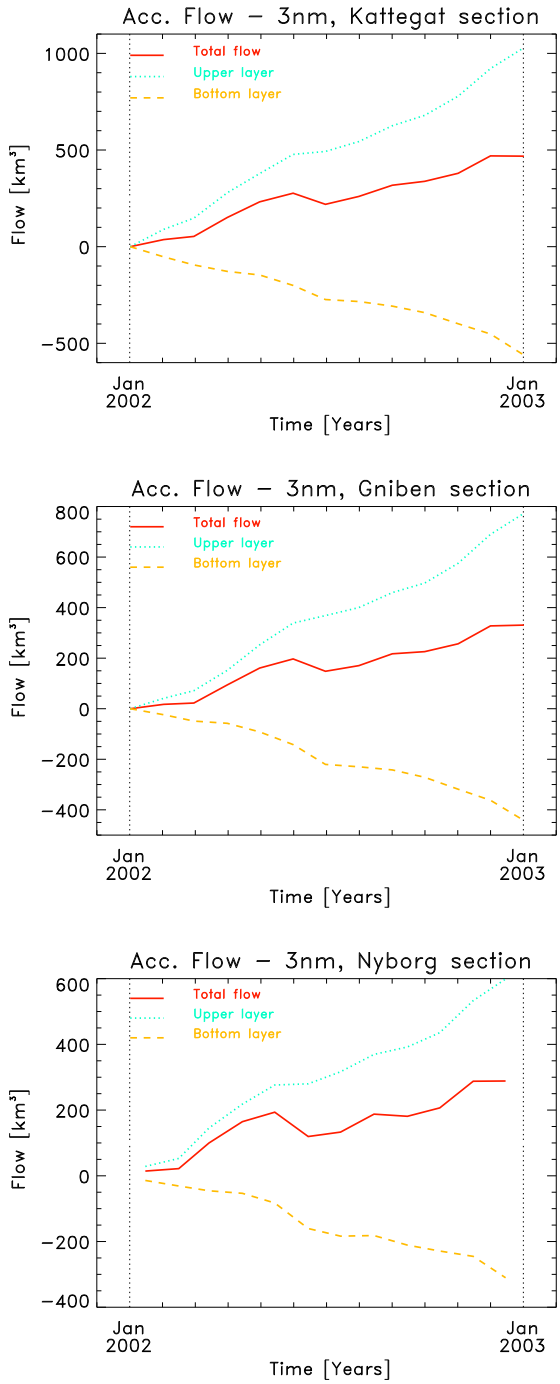

Fig. 30. Accumulated flow F_{acc} (monthly means) of the surface layer, bottom layer and entire water column from the GETM model, trough the sections Kattegat (upper panel), Gniben (middle panel) and Nyborg (lower panel).

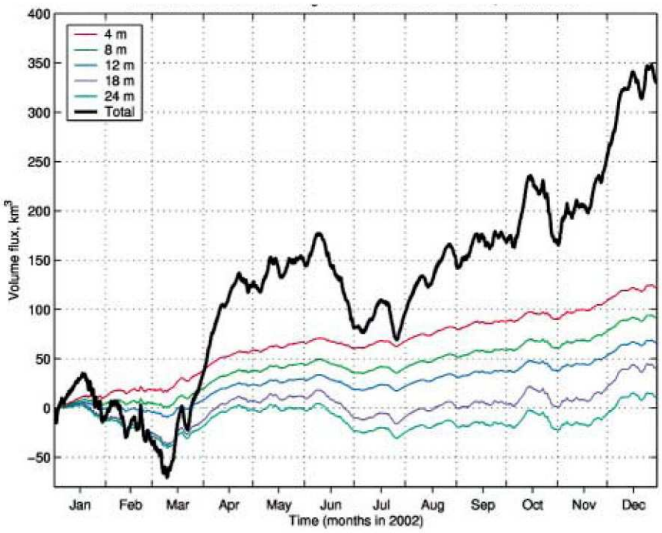

Fig. 31. Total accumulated flow trough the Gniben section (bold black line) and additionally flow at 5 different depth levels for the year 2002 calculated by the HIROMB model.

level in the Baltic Sea at the start of the modelled period and the runoff to the Baltic Sea during the year, as well as differences in the respective models performance and/or implementation.

Both models show that the total outflow was interrupted by periods of inflow from the Kattegat. The largest of these flow reversals occurred from the middle of January to the middle of March. Further to this, smaller flow reversals occurred at the end of April ($\sim$30 km^3), during June ($\sim$100 km^3) and at the end of October ($\sim$80 km^3). The periods immediately after these inflow events appear to have greater than average outflow.

The HIROMB data shows that the main outflow takes place in the upper 12 metres. The 18 metre layer (12-18 m) shows inflow and outflow to be balanced until the end of October. In the bottom layer, at 24 metres (18-24 m), inflow occurred from January to about March 10th, in the second half of June, and the second half of October. The first inflow was succeeded by outflow until the middle of April, followed by a calm period until the beginning of June. Only small volume changes occurred during the period from the end of July, until the beginning of October.

Figure 32 presents the absolute flow of the benthic layer for Gniben and Nyborg sections calculated by the JRC model from 1997 to 2002. Negative values indicate a southward flow from the Kattegat to the Belt Sea area. In agreement with the SMHI model, the JRC model (Gniben section) shows maxima of inflow to the Belt Sea for 2002 in February, June and December. Minima for 2002 are in March, July and August. Compared to other years, 2002 is mainly characterised by exceptional inflow in June and December and, above all, an

inflow minimum that lasted for an exceptionally long time during July-August in the Gniben section, with stagnation during August in the Nyborg section. This minimum of water exchange during summer months meant that there was poor oxygen supply to the bottom waters of the Belt Sea area, Summer water exchange in 1997 has similarities to 2002, although the inflow as a whole was substantially higher.

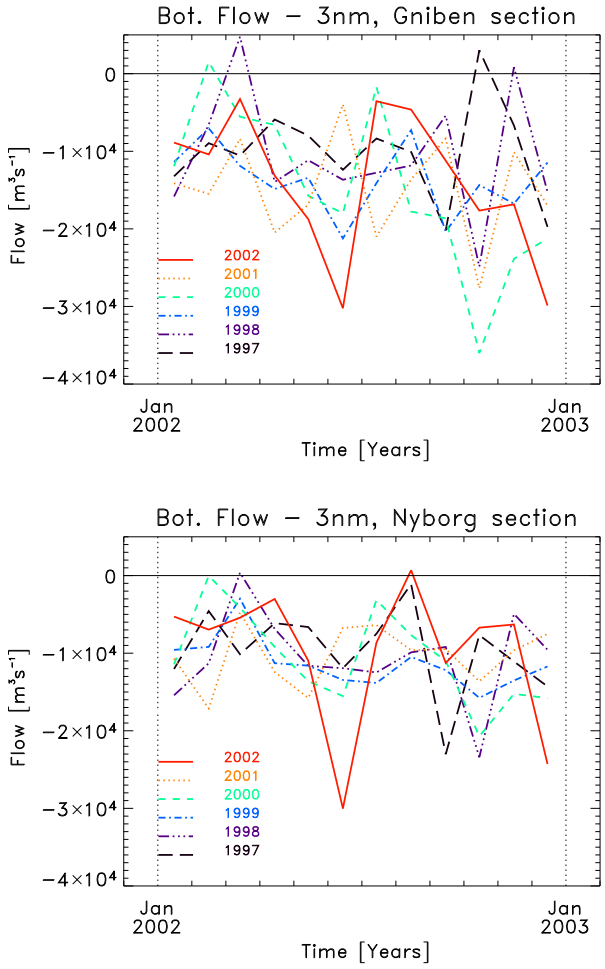

Fig. 32. Benthic layer flow for the Gniben section (upper panel) and the Nyborg section (lower panel) calculated by GETM from 1997 to 2002. Negative values indicate southward flow, from the Kattegat to the Belt Sea.

5.4.3 Discussion and summary

Two independent models showed good agreement describing the total inflow/outflow through the Belt Sea and the major flow variations in 2002. There were saline inflows to the Belt Sea and the Sound during June 2002, followed by increased brackish water outflow from the Baltic in July and especially in August, followed by a period of stagnation until the end of September.

The absolute inflow of the benthic layer estimated by the JRC GETM model suggests an exceptional inflow from the Kattegat in June 2002, which led to normal oxygen conditions near the bottom. The June inflow was followed by an inflow minimum in July-August through the Great Belt that lasted for two months, with stagnation in August in the Gniben section. The inflow was lower in July, October and November compared to other years. It is exceptional that these inflow minima and stagnation events were sustained for such a long period. The seasonal cycle of inflows from the Kattegat to the Belt Sea has a minimum (maximum residence time) during the summer. Stagnation events in 2002 appeared to be of a longer duration than observed in the previous four years of model data.

5.5.1 General analysis

Satellite data provides an independent source of spatial and temporal data coverage, which can be used for assessing the quality of performed simulations. To compare the model's Sea Surface Temperature (SST), to satellite observations of SST, we use monthly 4 km and 9 km AVHRR data from the NOAA/NASA Ocean Pathfinder satellite, see http://podaac.jpl.nasa.gov/sst. The 4 km data were chosen, since they have a similar horizontal resolution to the used fine model setup, whereas the 9 km data have a similar resolution to the coarse model setup. The accuracy of the satellite SST's is supposed to be in the order of about 0.5 K (Annan and Hargreaves (1999)).

First we present the mean SST anomaly for the total North Sea – Baltic Sea area in figure 33. For such a comparison, we must point out, that the SST calculated within GETM is no skin temperature, but rather the mean temperature of the uppermost model layer, having a thickness of about 2 m. On the other hand, also AVHRR data are often calibrated, using in-situ data instead of skin temperature data from infrared radiometers, and thereby also do not represent real skin SST. Further uncertainty is added to such comparisons by the problem of the diurnal thermocline, which builds up during sunny and calm days. In such situations the SST measured by the satellite will be about 1 – 2^{o}C higher than an situ temperature measured at some meters depth. This would lead to a positive bias in the AVHRR data, compared to the model data. In order to avoid such additional uncertainty, it is better to compare only night time satellite data and model data to each other, which is done in this study. From the time series in figure 33 we can see a good general agreement of the seasonal dynamics between the two data sets. Especially the winter temperatures correspond rather well to each other. The maximum temperature in summer of the AVHRR data is typically about 1^{o}C higher than the simulated SST. Performing a linear regression analysis of the total mean SST data, we find a significant trend in the data. The mean SST in the GETM data is increasing by 1.38^{o}C during the 13 year simulation, whereas the AVHRR temperature increases by about 1.18^{o}C. The annual increase of 0.11^{o}C/year (GETM) and 0.091^{o}C/year (AVHRR) is not significantly different (testing at the 99% level). This increasing tendency is statistically significant and in qualitative agreement with global trends for the last decade, which give a typical warming rate of about 0.1^{o}C/year.

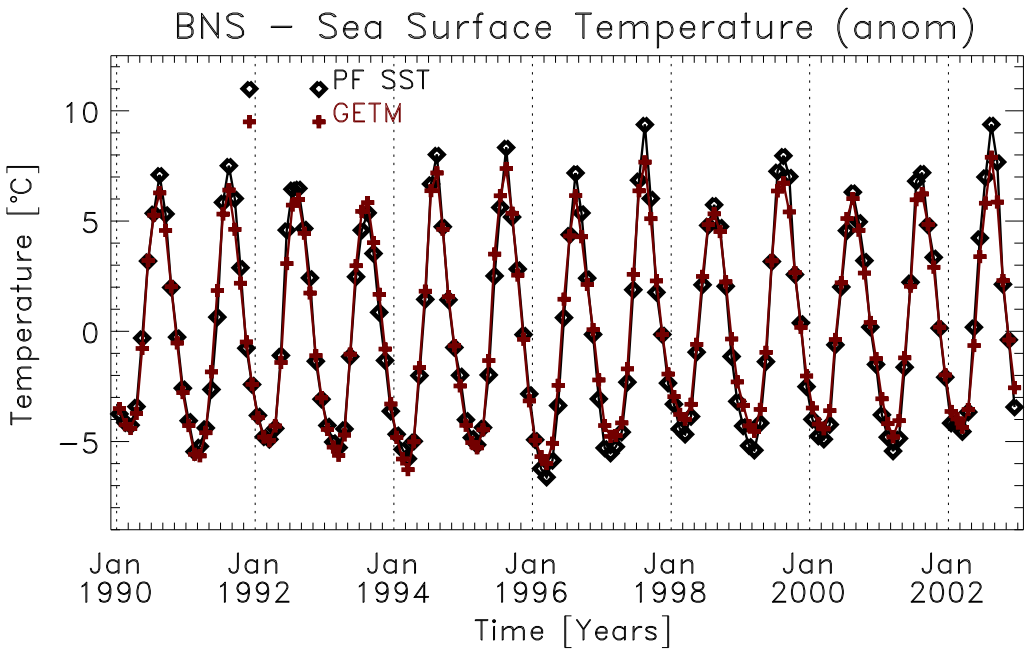

Fig. 33. Anomaly of the mean SST for the coupled North Sea – Baltic Sea system, derived from 9 km AVHRR data and the GETM coarse resolution simulation.

5.5.2 Regional variations of SST simulation

A realistic simulation of SST using 3D hydrodynamical models is very much dependent on the quality of the turbulence model used and of the applied advection schemes, both of which used within GETM are state of the art. The importance of the correct description of the short wave attenuation in the water column is often underestimated (there are still many models which prescribe the short wave radiation only as boundary condition for the uppermost layer). In GETM short wave radiation is absorbed following the parametrisation of Paulson and Simpson (1977) and selecting the appropriate Jerlov type for the water (Jerlov (1968)). This applied light absorption is constant in time and space, which might be justified for estuaries or small regions. In reality the light absorption over such large areas as the coupled North Sea – Baltic Sea system is varying spatially, but also in time. To demonstrate the influence of the chosen single water type for the overall model domain, we compare monthly model mixed layer temperatures to night time AVHRR SST for selected smaller regions.

In figure 34 the respective least square fits for the Baltic Sea and the North Sea areas are shown. We find that the slope of the regression lines for these areas is different (1.12 for the central North Sea and 0.94 for the Baltic Sea proper), pointing to the problem that the used common absorption coefficients are giving too high absorption in the North Sea and somewhat too small in

the Baltic Sea.

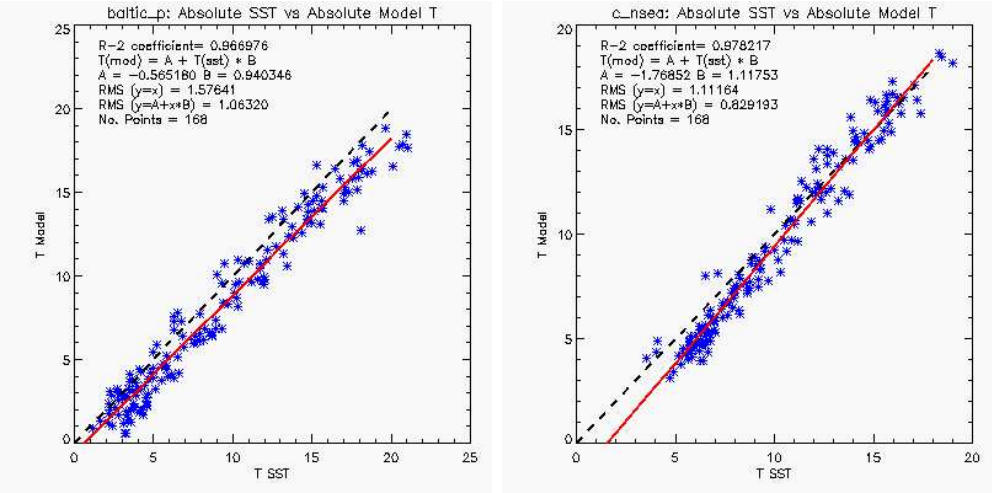

Fig. 34. Linear regression between mean AVHRR SST and mixed layer temperature for the Baltic Sea proper (left panel) and central North Sea (right panel), derived from 4 km AVHRR data and the GETM fine resolution simulation.

To test this hypothesis we will perform least square fits for regions having a higher absorption like coastal areas. The results of this analysis for the Gulf of Finland and the Gulf of Riga are shown in figure 35. Evidently the slope of the calculated regression curves is again smaller, which means that the simulated mixed layer temperature is underestimated in such more turbid areas, when compared to the open Baltic Sea.

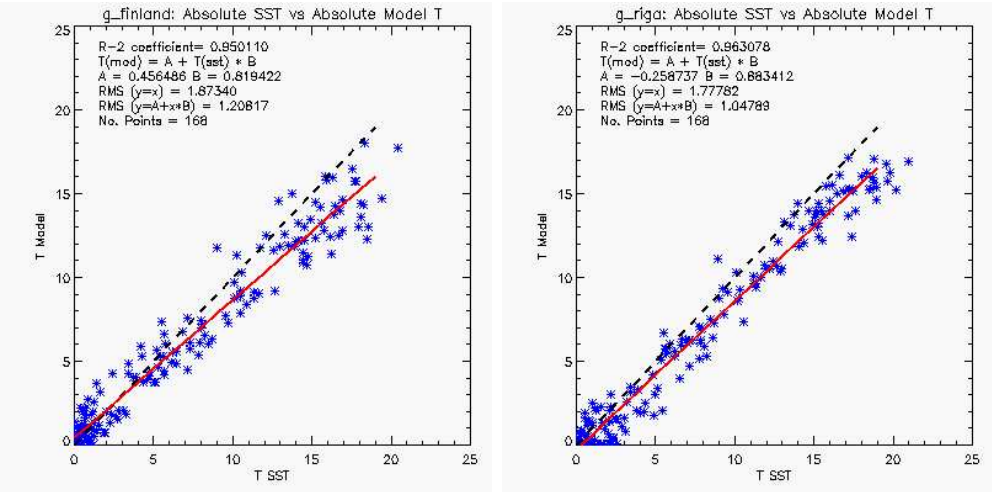

Fig. 35. Linear regression between mean AVHRR SST and mixed layer temperature for the Gulf of Finland (left panel) and Gulf of Riga (right panel), derived from 4 km AVHRR data and the GETM fine resolution simulation.

5.5.3 EOF analysis of SST

Calculation of empirical orthogonal functions (EOF's) is a useful technique for compressing the variability of spatial varying (e.g. maps) time series data. The EOF procedure is also called principal component analysis (PCA), or in social sciences factor analysis. The advantage of EOF analysis is that it provides a rather compact description of the spatial and temporal variability of a data set in terms of orthogonal functions. Thereby the variance of a spatially distributed time series is simply partitioned, without the need of a direct physical relationship between the derived statistical EOF's and any related dynamical modes to exist. Conventional EOF analysis can be only used to detect standing oscillations. Here we very briefly present some results of a preliminary EOF analysis of the coupled North Sea – Baltic Sea system. For the analysis of the whole model domain, SST data from the coarse model runs and monthly 9 km AVHRR data were used. Tests using data from the fine resolution model, showed that the EOF calculation for such a large dataset took more then 20 hours and we therefore refrained from doing this, until no final high quality data set for the analysis will be available.

The principal components for the time period from 1990 until 2002 resulting from this analysis are presented in figure 36. For this analysis the mean value was removed, but the seasonal cycle was left in the data. Therefore not surprisingly the very strong signal resulting from the seasonal cycle gives the largest contribution to the overall variance. For a more detailed analysis the seasonal signal should be removed beforehand. Nevertheless there is an evident difference between the principal components from GETM SST and from AVHRR SST, namely the contribution to the variance from the higher principal components (1,2,3) of the AVHRR SST is practically vanishing, whereas for the GETM SST, there are still significant contributions until the 3rd principal component. We do not have a real satisfactory explanation for this behaviour, especially as we would expect also higher principal components to be present in the AVHRR SST data.

The calculated spatial variability of the first orthogonal eigenfunction (EOF0) is shown in figure 37. We can identify the pronounced West-East gradient as the prominent feature in figure 37. The first EOF's from model and from SST data are both determined by the seasonal variability, therefore they both show similar spatial patterns to each other.

The results for the second EOF differ already considerably between the simulations and the AVHRR data (figure 38). The spatial pattern for the GETM EOF1 is characterised by a strong North – South gradient, whereas the AVHRR EOF1 shows a West – East variability with a maximum at about 10^o E. Obviously they must be related to different physical processes in the original data and cannot be compared directly. An improved EOF analysis should be performed, when simulated SST data using an improved model component for the short wave attenuation will be available. The interpolation of the AVHRR data must be also improved, see new approaches for filling in missing data by Alvera-Azcarate et al. (2004).

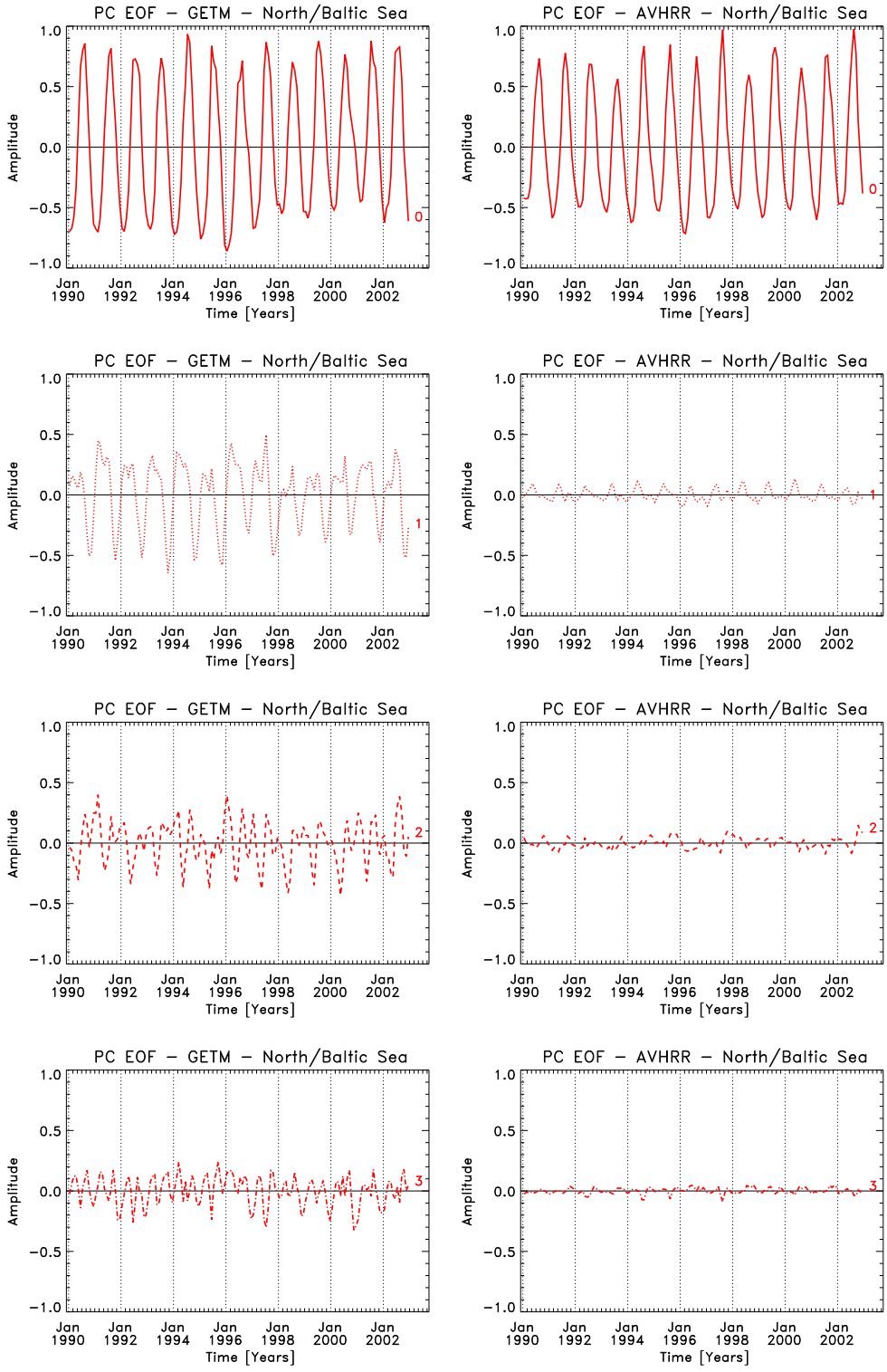

Fig. 36. Principal components for the SST of the coupled North Sea – Baltic Sea system, derived from 9 km AVHRR data and the GETM coarse resolution simulation.

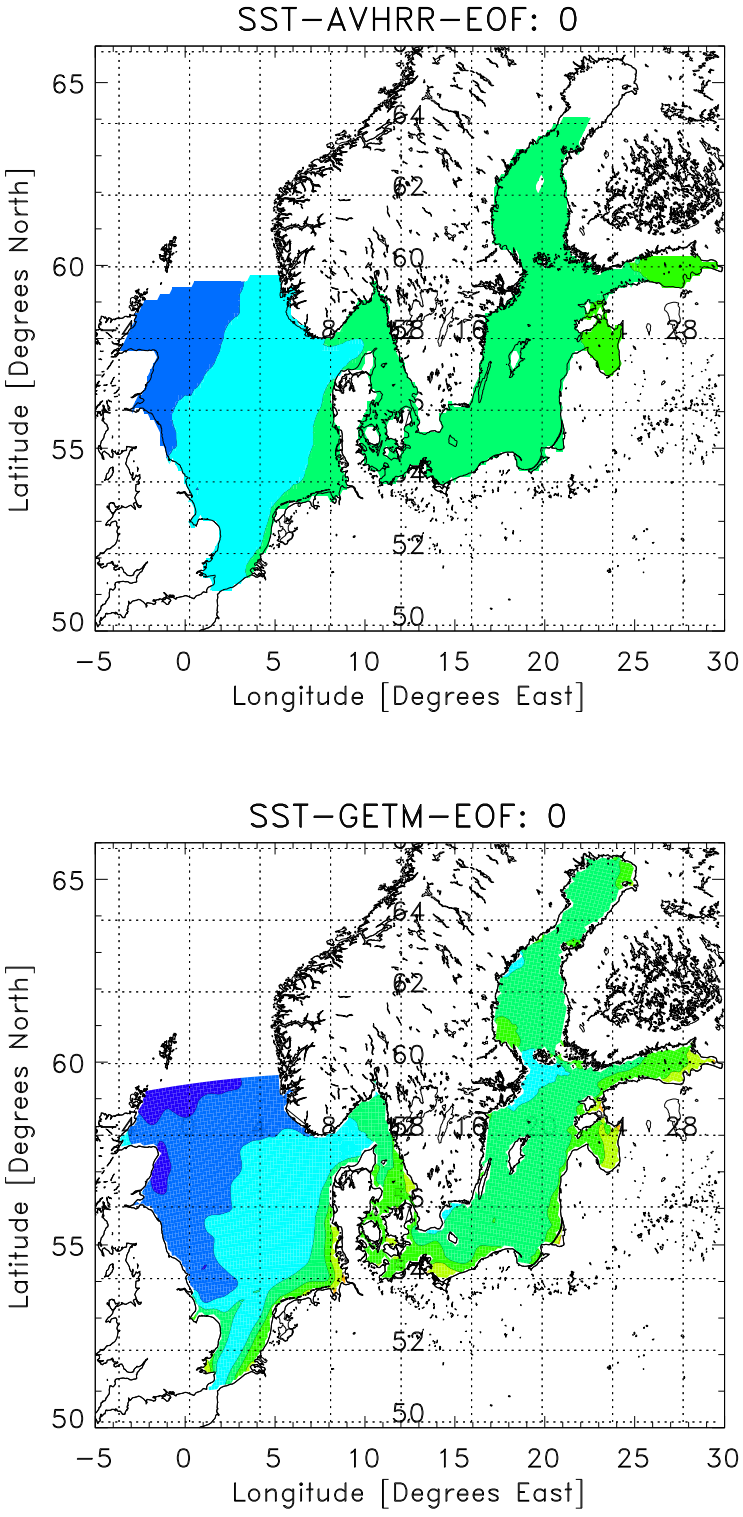

Fig. 37. First EOF for the SST of the coupled North Sea – Baltic Sea system, derived from 9 km AVHRR data (upper panel) and the GETM coarse resolution simulation (lower panel).

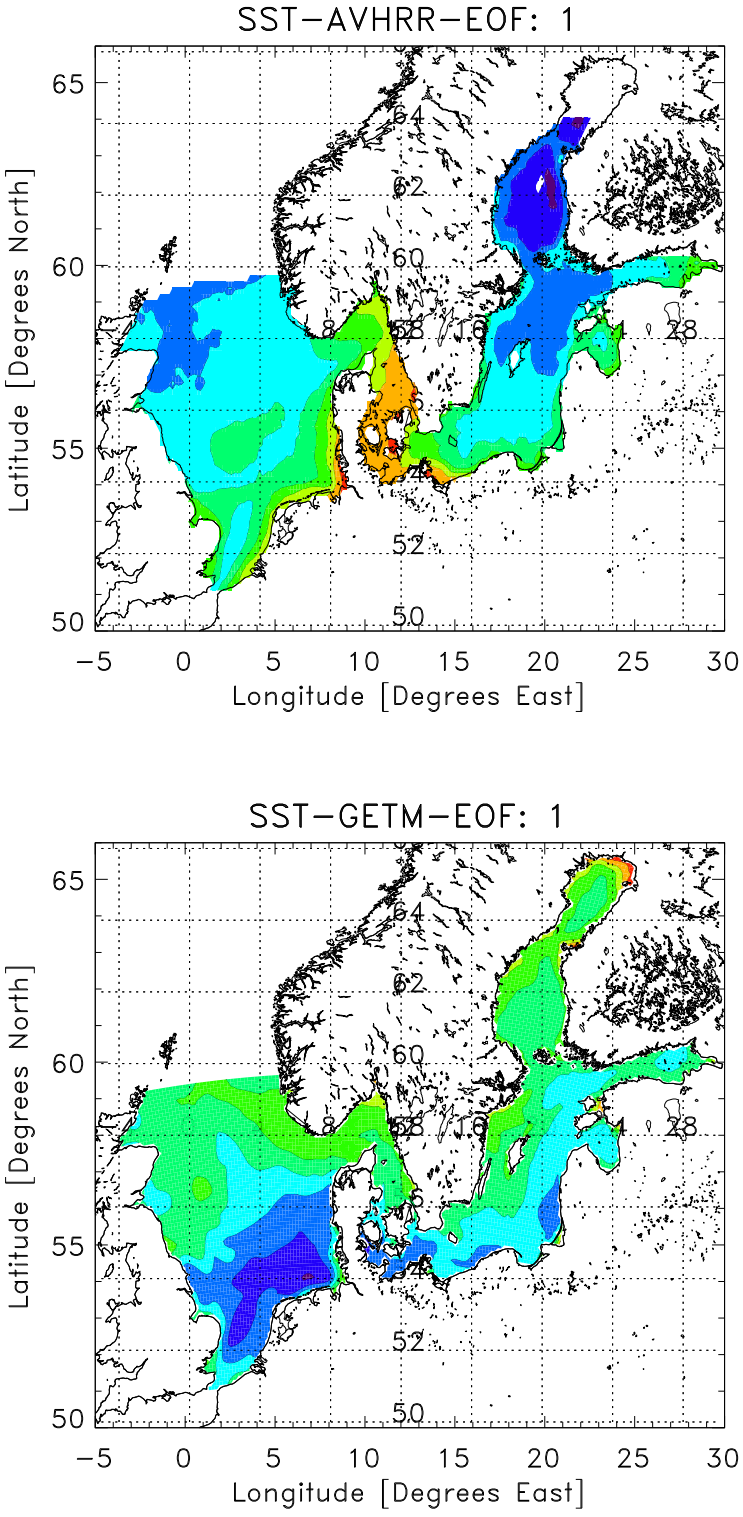

Fig. 38. Second EOF for the SST of the coupled North Sea – Baltic Sea system, derived from 9 km AVHRR data (upper panel) and the GETM coarse resolution simulation (lower panel).

5.6 Development of a physical indicator (PSA)

To improve the assessment and management of water quality in European Regional Seas there is a need to develop indicators which provide a simplified, but still scientificly correct, and comprehensive, picture of the physical status of the marine environment. Such known indicators are e.g. the residence time (or flushing time) of an aquatic system. The residence time describes the expected mean time a certain particle will remain in the considered control volume (e.g. an estuary). It is obvious that the residence time is a compact indicator, which describes only certain characteristics of the system, without giving a comprehensive description. Therefore work at the JRC was devoted to the development of a more comprehensive indicator, which should consider also such important features as vertical stratification. The result of this development is the Physical Sensitive Area (PSA) index, which is described in detail in Druon et al. (2004) and Djavidnia et al. (2004). Most important physical factors which are considered in the PSA are the Mixed layer Depth (MLD), the maximum of the density gradient, bottom friction, the current velocities, temperatures and salinities. Velocities, temperatures and salinities are separated in bottom layer and in the surface layer values. Without dealing with the details of the PSA indicator, we want to present selected results for parameters, which had to be derived from the model data for finally calculating the PSA indicator.

Multi-annual realistic simulations of the coupled North Sea – Baltic Sea system were performed to derive monthly mean values for each of the needed PSA input parameters. From these 12 to 17 year long time series, climatological mean values for every month were calculated and finally used for the PSA indicator. Of course the availability of such multi-annual time series of important physical parameters will also allow the analysis of trends within the data, but this will be the aim of a separate report.

Results for calculated monthly mean surface currents and the corresponding MLD for the year 1997 are shown in figure 39 and figure 40. The MLD typically has a minimum in summer and a maximum value during winter, when convection destroys the stratification. Regions of fresh water influence (see the river outflow from the Rhine) are practically permanently stratified. Coastal currents are usually stronger than currents in the open sea. Note the characteristic cyclonic circulation in the Gotland Sea during most of the year.

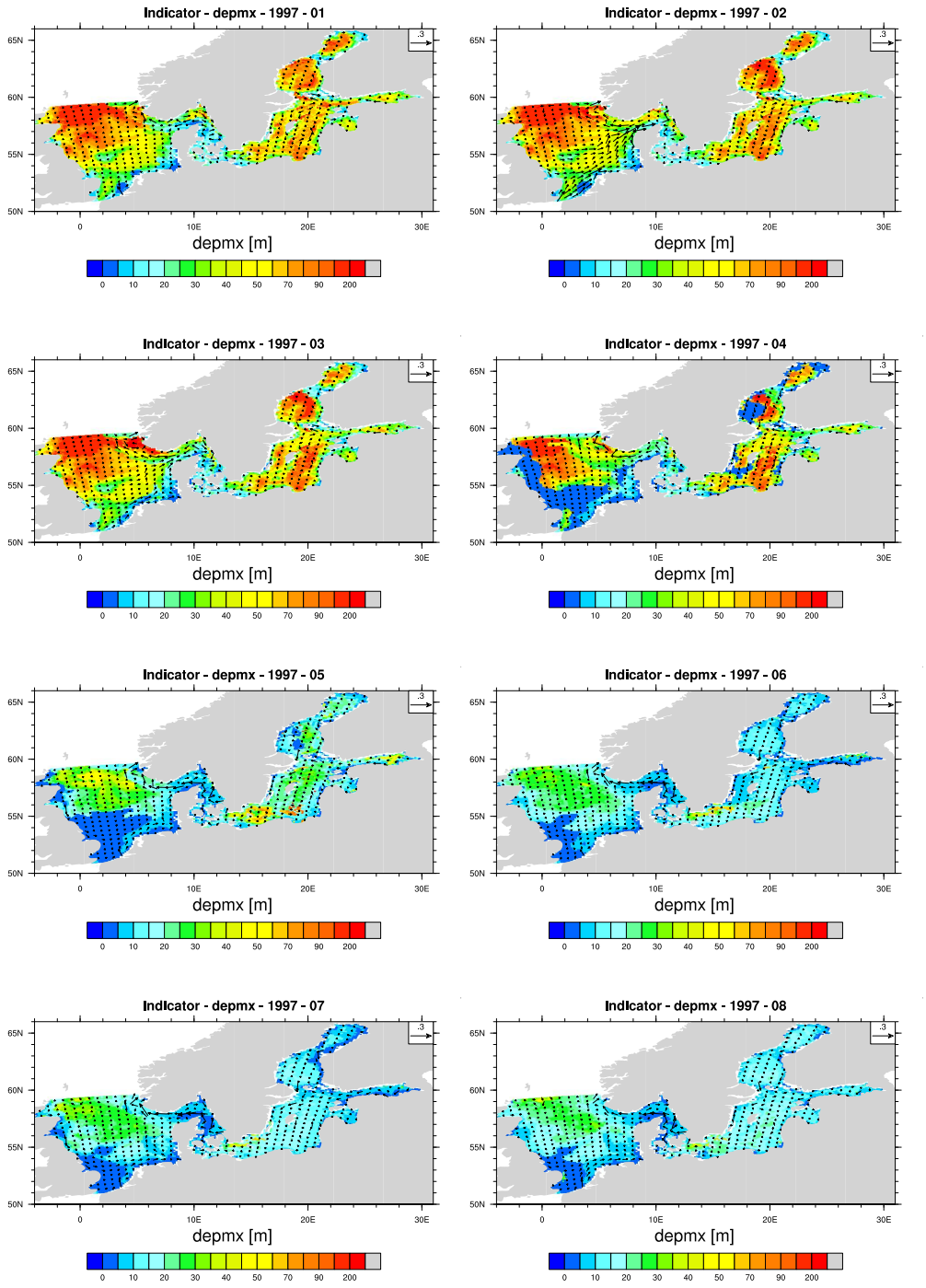

Fig. 39. Contour plots of monthly mean values of the Mixed Layer Depth and mixed layer velocities in the North Sea and Baltic Sea during 1997.

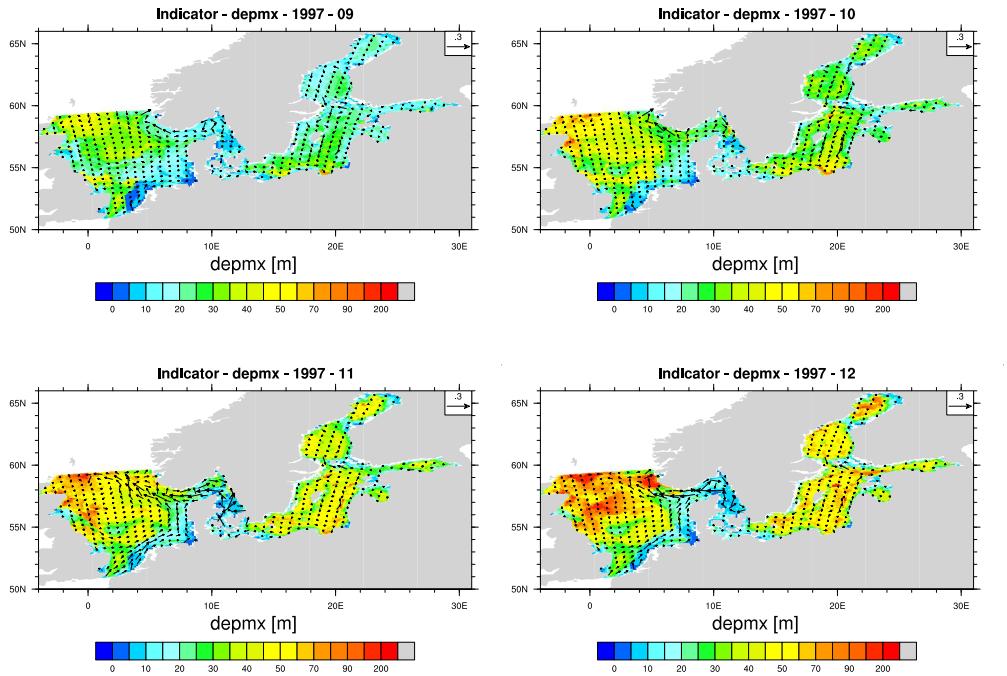

Fig. 40. Continuation of contour plots of monthly mean values of the Mixed Layer Depth and mixed layer velocities in the North Sea and Baltic Sea during 1997.

As stated before, the results for the single months from the multi-annual simulation were finally averaged together to construct a monthly climatology. The calculated climatology for the surface layer temperature is shown in figure 41. The annual cycle of cooling until March, then warming until July and again cooling is clearly visible. The strong North – South gradient, which is persisting throughout the year is also apparent. Shallow areas are typically cooler in winter and warmer in summer compared to adjacent deeper areas.

The surface layer salinity climatology for the North Sea (figure 42) exhibits strong signs of river plumes from Rhine and Elbe, having reduced salinities over long distances away from the river mouth. Further to this the quasi permanent outflow of less saline Baltic Sea surface water along the Norwegian coasts can be identified in the simulations.

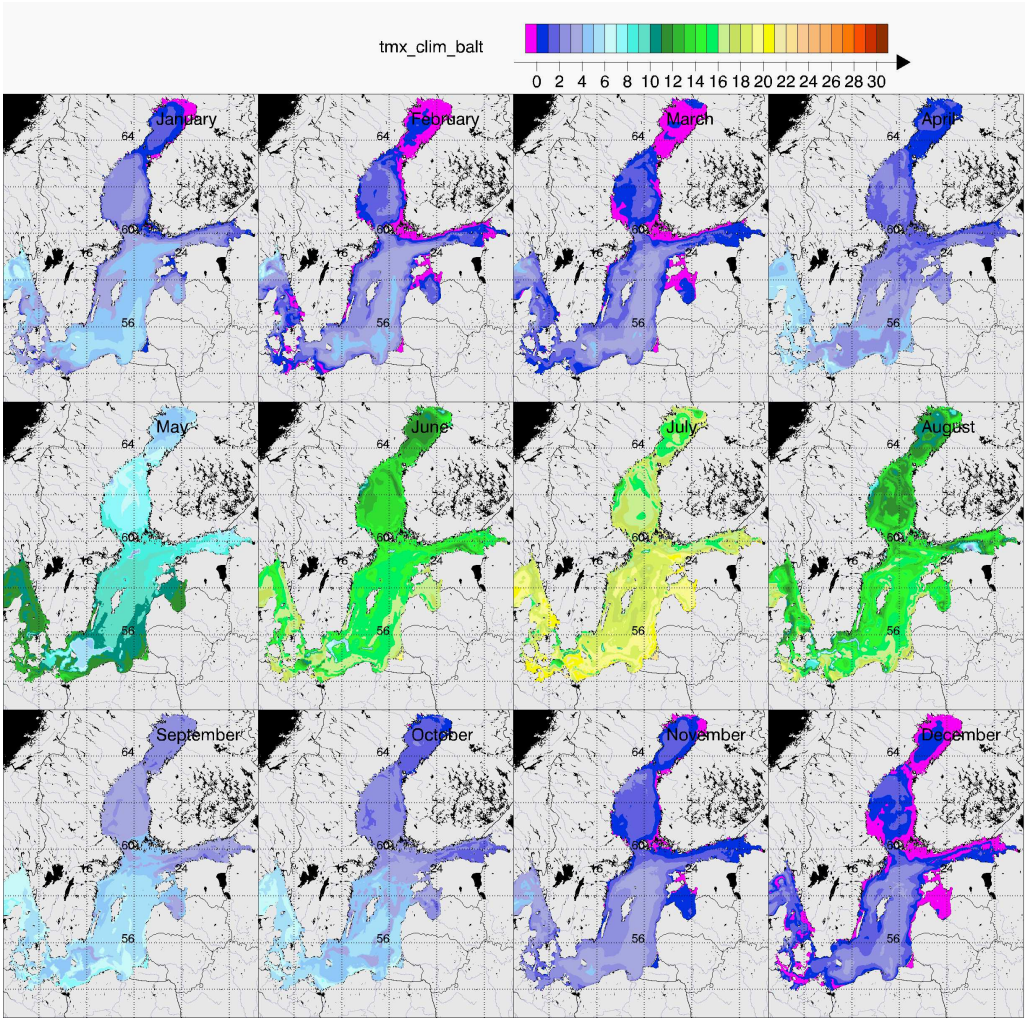

Fig. 41. Monthly climatology of surface layer temperature for the Baltic Sea. The annual cycle of cooling and warming as well as the pronounced North - South gradient of temperature is evident.

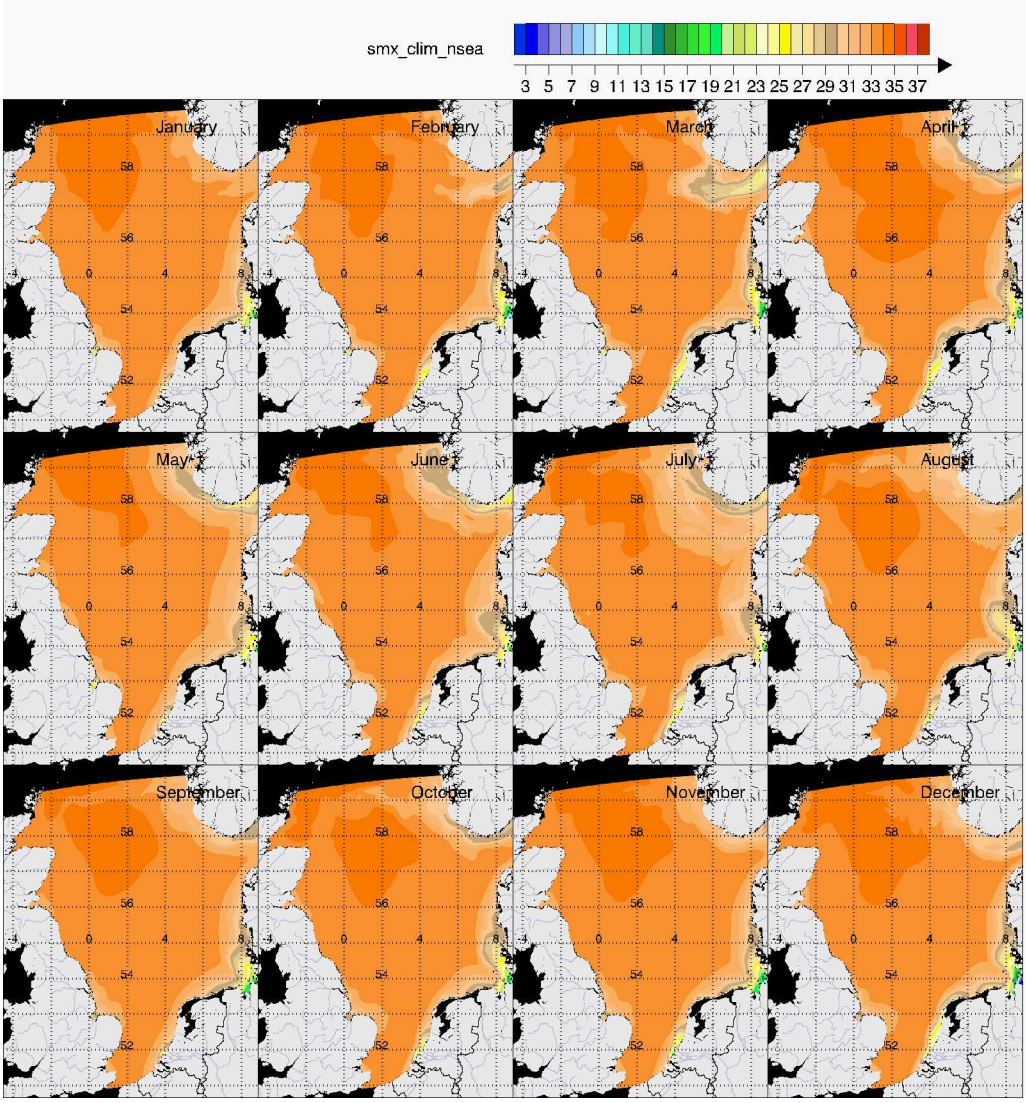

Fig. 42. Monthly climatology of surface layer salinity for the North Sea. Reduced salinities in coastal areas due to river outflow or outflow from the Baltic Sea can be identified.

6 Conclusions

Here we could demonstrate that over many other models, GETM has several advantages:

- **Numerical stability:** During all simulations on spherical and on cartesian grids, the high numerical stability of GETM was evident. The 3 nm $\times$ 3 nm annual simulations of the coupled North Sea - Baltic Sea system were carried out with a baroclinic time step of about 15 minutes. Considering the maximum water depth of more than 700 m, which means a Courant number of about 20 for the barotropic surface waves, this is achieved here with an external micro time step of about half the Courant number and a large split factor between baroclinic and barotropic mode of $M = 30$. Importantly, no smoothing by explicit horizontal diffusion and no filtering needs to be applied, methods which are frequently used in many other models. The reasons for this good model performance of GETM are the careful coupling of the barotropic and the baroclinic mode and the high-order advection schemes which guarantee positivity without any filtering.
- **High-order advection:** There are several high-order advection schemes implemented into GETM, which are all based on the principle of finite volumes. This guarantees conservation of mass and heat down to the level of machine-accuracy. Furthermore, these schemes are inherently monotone, which means that they do not artificially generate any oscillations. Thus no filtering or smoothing of the model results is needed. Due to these characteristics, meso-scale features are visible in the model results even for the coarse-resolution simulation on the 6 nm $\times$ 6 nm cartesian grid. The trade-off for such advanced schemes is higher computational time in comparison to upstream or centred differences.
- **High-order turbulence models:** One of the classical advantages of GETM is the coupling with the turbulence module of GOTM, the General Ocean Turbulence Model. This allows for choosing the optimal turbulence closure scheme for any simulation. There are different levels of complexity available, ranging from simple one-equation models to complex two-equation models with algebraic second-moment closures. In the present simulations, a compromise between accuracy and complexity was chosen, the two-equation standard k-ε model.
- **Flexible vertical coordinates:** One further strength of GETM is the use of general vertical coordinates. In contrast to σ coordinates, this allows for layer thicknesses which are horizontally homogeneous near the surface and also near the bed. However, in the present state of GETM, the number of layers is fixed in all horizontal points, no matter how deep the water is. Thus, geopotential coordinates as used in many models for the Baltic Sea, are not yet included, see below.

- **Curvy-linear coordinates:** The use of orthogonal curvy-linear coordinates which allow zooming of grid boxes in areas of special interest, is one of the features of GETM which could be very advantageous for future projects. It allows for high resolution in the area of the Danish Straits with their complex bathymetry without model nesting. The potential of the curvy-linear coordinates requires further investigation.
- **Parallelisation:** The GETM code is now fully functional in parallel mode. As the implementation was targeted to distributed memory systems (as e.g. the actual LINUX cluster built up at the IMW unit) the domain decomposition method using the Message Passing Interface (MPI) protocol has been used for transferring data between different sub-domains.
- **Modular structure:** The modular structure of GETM allows for easy implementation of further processes. In the moment, the coupling with a surface wave module and a Lagrangian particle module is in the testing phase, and will be used for oil spill modelling. The coupling of GETM with different ecosystem models is also under development. Further modules which could be added to GETM in the future would be a sea ice module and a wave model.

There are a few features which are yet missing in GETM or at least need further consideration. It should however be noted that none of these missing features is in conflict with the general structure of GETM. The features which need to be considered in the future are:

- **Light absorption** One question which is closely related to the suitable turbulence model is the model for light absorption in the water column. Here, we have used a mixture of Jerlov oceanic class III and coastal class 3 water, which is surely a simplification since in spring and summer plankton blooms strongly increase the turbidity. Therefore the spatial and temporal variation of light absorption should be considered in the future. Thus, the mixed layer depth predicted in the present study might be overestimated/underestimated and consequently the sea surface temperature underestimated/overestimated in summer. First model tests using spatial and temporal varying attentuation coefficients are doen for the Black Sea.
- **Sea ice model:** Currently, the effect of sea ice which is extensively occurring in the Northern parts of the Baltic Sea is parameterised by simply setting the minimum surface temperature to the melting point. This seems to be sufficient as long as the focus of investigations is on the Danish Straits, as for the salt water exchange studies done here. However, much of the dynamics of the Baltic Sea would be more realistic with the proper consideration of sea ice. There are several Public Domain versions of sea ice models such as the Hibler (1979), Hibler (1985) type models available.
- **Consideration of convection:** During extended time periods convection plays an important role for de-stratifying the water column and generating deep mixing. The here applied turbulence model does not explicitely con-

sider convective processes, it rather provides an implicit parameterisation of convection. As progress in turbulence modelling is to be expected, such improved vertical mixing parameterisations should give better results for the vertical density structure in the Baltic Sea.

- **Horizontal mixing** Horizontal diffusion is typically implicitly considered in 3D circulation models, because of numerical diffusion as e.g. introduced by applying rather diffusive advection schemes (like upstream advection) or by explicitly introducing horizontal constant diffusion, as done in GETM. Still, for some purposes improved horizontal diffusion parameterisations as e.g. a Smagorinsky type diffusion could be beneficial and should be included in the model options.
- **Two way nesting** Due to limited memory and computing resources it is not always possible to use very high grid resolution for very large model domains. In order to have the full dynamics available when simulating small estuaries or bays with very high resolution, while the greater domain has a coarse resolution, two way nesting has to be applied. In this case information is passed from the larger domain to the smaller (higher resolved) and vice versa. As it is shown, that the applied 3 nm $\times$ 3 nm resolution is too coarse for resolving the details of the water transport trough the Danish Straits, such a two way nesting is urgently needed for higher quality simulations, with still acceptable computational effort.
- **Improvement of vertical coordinates:** One major problem to be solved in the future is the excessive vertical mixing, which occurs over steep topographic features. This results in the drainage of salinity from the deep basins, observed especially in the Gotland Deep. This is surely related to the choice of the coordinate system which results in too steep coordinate slopes. Compared to the initial results from 2002, during the last 2 years considerable progress in this matter has been made, mainly by carefully smoothing bathymetric features and by selecting specific distributions of the vertical co-ordinates, see section 5.3. There are many numerical investigations which try to solve this problem by improving the discretisation of the internal pressure gradient calculation. However, real breaktroughs have not been achieved yet, and can maybe not be expected. Therefore, other techniques have to be discussed. One simple way would be to go back to geopotential coordinates. This type of coordinates has however a number of disadvantages, such as the bad representation of dense bottom plumes and the low vertical resolution over sills. The latter, especially in the Baltic Sea, play a key role in understanding the overall dynamics. A future task would be to develop a hybrid coordinate system which does not have the disadvantages of either of the other coordinate systems. Some realisations have been suggested in the past, see e.g. Beckers (1991), Gerdes (1993), Burchard and Petersen (1997) and Bleck (2002) and the discussion in the introduction of this report. Finding such a coordinate transformation is surely a scientific task of high priority.

7 Acknowledgement

Many European scientists and institutions contributed to this study by either providing data, discussing problems and results or giving important advice, we would like to thank all of them. Nevertheless, due to their extraordinary efforts many reward a more detailed mentioning of what they did to us. We would like to thank Thomas Pohlmann and Roger Proctor for helping to compare our first realistic model results to model simulations performed by the NOMADS2 consortium and specifically at Hamburg university using the HAMSOM model. The oxygen depletion study in the Kattegat Belt Sea area was performed in the framework of a special HELCOM project, together with Gunni Aertebjerg (NERI, Denmark) and Philipp Axe (SMHI, Sweden), who also provided the HIROMB flow data. Without the extremly helpful and beneficial support from the European Centre for Medium Term Weather Forecasting (ECMWF), which provided access to all their meteorological analysis and reanalysis (ERA40) data never the good and realistic level of the performed multiannual simulations would have been reached. Tidal gauge data from Danish stations were kindly provided by Palle Bo Nielsen from the Royal Danish Administration of Navigation and Hydrography (Farvandsvæsenet). Satellite AVHRR sea surface data were made freely available by the National Oceanic and Atmospheric Administration (NOAA, US). Thomas Neumann (IOW) provided climatological river data and data for selected monitoring stations in the Baltic Sea. The meteorological data for the very coarse resolution simulation of the North Sea were provided by the UK-Met Office. This work was done within the institutional project ECOMAR (2121) in framework programme FP6, supported by the JRC programme directorat and DG Environment.

References

Aertebjerg, G., Hansen, J., Axe, P., Druon, J.-N., Stips, A., 2003. The 2002 oxygen depletion event in the Kattegat, Belt Sea and Western Baltic. Tech. Rep. Baltic Sea Environment Proceedings No. 90, Helsinki Commission, Baltic Marine Environment Protection Commission, Helsinki, Finland.

Alvera-Azcarate, A., Barth, A., Rixen, M., Beckers, J. M., 2004. Reconstruction of incomplete oceanographic data sets using empirical orthogonal functions: application to the Adriatic Sea surface temperature. Ocean Modelling xxx, xxx–xxx.

Annan, J. D., Hargreaves, J. C., 1999. Sea surface temperature assimilation for a three-dimensional baroclinic model of shelf seas. Cont. Shelf Res. 19, 1507–1520.

Backhaus, J. O., 1985. A three-dimensional model for simulation of shelf sea dynamics. Dt. Hydrogr. Z. 38, 165–187.

Beckers, J.-M., 1991. Application of a 3D model to the Western Mediterranean. J. Mar. Sys. 1, 315–332.

Beckmann, A., Döscher, R., 1997. A method for improved representations of dense water spreading in geopotential coordinate models. J. Phys. Oceanogr. 27, 581–591.

Bleck, R., 2002. An oceanic general circulation model framed in hybrid isopycnic-cartesian coordinates. Ocean Modelling 4, 55–88.

Blumberg, A. F., Mellor, G. L., 1987. A description of a coastal ocean circulation model. In: Heaps, N. S. (Ed.), Three dimensional ocean models. American Geophysical Union, Washington, D.C., pp. 1–16.

Bolding, K., Burchard, H., Pohlmann, T., Stips, A., 2002. Turbulent mixing in the Northern North Sea: a numerical model study. Cont. Shelf Res. 22, 2707–2724.

Bryan, K., 1969. A numerical model for the study of the world ocean. J. Computat. Phys. 4, 347–376.

Burchard, H., 2001a. Simulating the wave-enhanced layer under breaking surface waves with two-equation turbulence models. J. Phys. Oceanogr. 31, 3133–3145.

Burchard, H., 2001b. Simulating the wave-enhanced layer under breaking surface waves with two-equation turbulence models. J. Phys. Oceanogr. 31, 3133–3145.

Burchard, H., 2002. Applied turbulence modelling in marine waters. Vol. 100 of Lecture Notes in Earth Sciences. Springer, Berlin, Heidelberg, New York.

Burchard, H., Bolding, K., 2002. GETM, a general estuarine transport model. Scientific documentation. Tech. Rep. EUR 20253, European Commsission, Ispra.

Burchard, H., Bolding, K., Rippeth, T. P., Stips, A., Simpson, J. H., Sündermann, J., 2002. Microstructure of turbulence in the Northern North Sea: A comparative study of observations and model simulations. Journal of Sea Research 47, 223–238.

Burchard, H., Bolding, K., Villarreal, M. R., 1999. GOTM – a general ocean turbulence model. Theory, applications and test cases. Tech. Rep. EUR 18745 EN, European Commission.

Burchard, H., Petersen, O., 1997. Hybridisation between σ and z coordinates for improving the internal pressure gradient calculation in marine models with steep bottom slopes. Int. J. Numer. Methods in Fluids 25, 1003–1023.

Canuto, V. M., Howard, A., Cheng, Y., Dubovikov, M. S., 2001. Ocean turbulence. Part I: One-point closure model - Momentum and heat vertical diffusivities. J. Phys. Oceanogr. 31, 1413–1426.

Cox, M. D., 1984. A primitive equation, 3-dimensional model for the ocean. Tech. Rep. 1, Geophysical Fluid Dynamics Laboratory, University of Princeton, Princeton, N. J.

Craig, P. D., 1996. Velocity profiles and surface roughness under breaking

waves. J. Geophys. Res. 101, 1265–1277.
Craig, P. D., Banner, M. L., 1994. Modelling wave-enhanced turbulence in the ocean surface layer. J. Phys. Oceanogr. 24, 2546–2559.
Delhez, E. J. M., Damm, P., de Goede, E., de Kok, J., Dumas, F., Gerritsen, H., Jones, J. E., Ozer, J., Pohlmann, T., Rasch, P. S., Skogen, M., Proctor, R., 2004. Variability of shelf-seas hydrodynamic models: lessons from the NOMADS2 project. J. Mar. Sys. 45, 39–53.
Djavidnia, S., Druon, J.-N., Schrimpf, W., Stips, A. K., Peneva, E., Dobricic, S., Vogt, P., 2004. Oxygen Depletion RiskIindices - OXYRISK & PSA V2.0: New developments, stucture and software content. Tech. Rep. EUR xxxx, CEC Joint Research Centre, Ispra, Italy.
Druon, J. N., Schrimpf, W., Dobricic, S., Stips, A., 2004. Comparative assessment of large-scale marine eutrophication: North Sea area and Adriatic Sea as case studies. Marine Ecology Progress Series 272, 1–23.
Feistel, R., Nausch, G., Heene, T., Piechura, J., Hagen, E., 2004. Evidence for a warm water inflow into the Baltic Proper in summer 2003. Oceanologia 46, 581–598.
Fofonoff, N. P., Millard, R. C., 1983. Algorithms for computation of fundamental properties of sea water. UNESCO Technical Papers in Marine Science 44, 1–53.
Funkquist, L., Kleine, E., 1995. Application of the BSH model to Kattegat and Skagerak. Tech. Rep. RO 22, Swedish Meteorological and Hydrological Institute, Norrköping, Sweden.
Funkquist, L., Kleine, E., 2002. An introduction to an operational baroclinic model for the North Sea and Baltic Sea. Tech. Rep. RO 28, Swedish Meteorological and Hydrological Institute, Norrköping, Sweden.
Gerdes, R., 1993. A primitive equation ocean circulation model using a general vertical coordinate transformation. 1. Description and testing of the model. J. Geophys. Res. 98, 14683–14701.
Gustafsson, B. G., Andersson, H. C., 2001. Modeling the exchange of the Baltic Sea from the meridional atmospheric pressure difference across the North Sea. JGR 106, 19731–19744.
Haidvogel, D. B., Beckmann, A., 1999. Numerical Ocean Circulation Modelling. Vol. 2 of Series on Environmental Science and Management. Imperial College Press, London.
Haney, R. L., 1991. On the pressure gradient force over steep topography in sigma coordinate ocen models. J. Phys. Oceanogr. 21, 610–619.
Hibler, W. D., 1979. A dynamic thermodynamic sea ice model. J. Phys. Oceanogr. 9, 815–846.
Hibler, W. D., 1985. Modeling sea ice dynamics. Adv. Geophys. 28, 549–580.
Holt, J. T., James, I. D., 2001. An s coordinate density evolving model of the northwest European continental shelf 1, Model description and density structure. J. Geophys. Res. 106, 14015–14034.
Janssen, F., Schrum, C., Backhaus, J., 1999. A climatological dataset of temperature and salinity for the North Sea and the Baltic Sea. Dt. Hydrogr. Z.

9, 245–.
Jerlov, N. G., 1968. Optical oceanography. Elsevier.
Kantha, L. H., Clayson, C. A., 2000. Numerical models of oceans and oceanic processes. Vol. 66 of International Geophysics Series. Academic Press.
Kleine, E., 1994. Das operationelle Modell des BSH für Nordsee und Ostsee. Tech. rep., Bundesamt für Seeschiffahrt und Hydrographie, Hamburg, Germany.
Kondo, J., 1975. Air-sea bulk transfer coefficients in diabatic conditions. Bound. Layer Meteor. 9, 91–112.
Launder, B. E., Reece, G. J., Rodi, W., 1975. Progress in the development of a reynolds-stress turbulence closure. J. Fluid Mech. 68, 537–566.
Launder, B. E., Spalding, D. B., 1972. Mathematical models of turbulence. Academic Press, New York.
Lehmann, A., 1995. A three-dimensional baroclinic eddy-resolving model of the baltic sea. Tellus 47A, 1013–1031.
Lowry, R. K., Cramer, R. N., Rickards, L. J., 1992. North Sea Project. Tech. rep., British Oceanographic Data Centre, nERC CD-ROM.
Luyten, P. J., Deleersnijder, E., Ozer, J., Ruddick, K. G., 1996. Presentation of a family of turbulence closure models for stratified shallow water flows and preliminary application to the Rhine outflow region. Cont. Shelf Res. 16, 101–130.
Matthäus, W., Lass, H. U., 1995. The recent inflow into the Baltic Sea. J. Phys. Oceanogr. 25, 280–286.
Meier, H. E. M., 2000. The use of the k-ε turbulence model within the Rossby Centre regional ocean climate model: parameterisation, development and results. Tech. Rep. 28, Swedish Meteorological and Hydrological Institute, Norrköping, Sweden.
Meier, H. E. M., 2001. The first Rossby Centre regional climate scenario for the Baltic Sea using a 3D coupled ice-ocean model. Tech. Rep. RMK 95, Swedish Meteorological and Hydrological Institute, Norrköping, Sweden.
Mellor, G. L., Yamada, T., 1974. A hierarchy of turbulence closure models for planetary boundary layers. Journal of Atmospheric Sciences 31, 1791–1806.
Mellor, G. L., Yamada, T., 1982. Development of a turbulence closure model for geophysical fluid problems. Rev. Geophys. Space Phys. 20, 851–875.
Omstedt, A., Nyberg, L., 1994. A coupled ice-ocean model supporting winter navigation in the Baltic Sea.Part II: Thermodynamics and meteorological coupling. Tech. Rep. RO 21, Swedish Meteorological and Hydrological Institute, Norrköping, Sweden.
Omstedt, A., Nyberg, L., Leppäranta, M., 1994. A coupled ice-ocean model supporting winter navigation in the Baltic Sea.Part I: Ice dynamics and water levels. Tech. Rep. RO 17, Swedish Meteorological and Hydrological Institute, Norrköping, Sweden.
Paulson, C. A., Simpson, J. J., 1977. Irradiance measurements in the upper ocean. J. Phys. Oceanogr. 7, 952–956.
Pedlosky, J., 1987. Geophysical fluid mechanics, 2nd Edition. Springer, New

York.

Perrels, P. A. J., Karelse, M., 1982. A two-dimensional, laterally averaged model for salt intrusion in estuaries. Tech. Rep. Tech. Rep. 262, Waterloopkundig Laboratorium, Delft Hydraulics, Delft, Netherlands.

Proctor, R., Damm, P., Delhez, E., Dumas, F., Gerritsen, H., de Goede, E., Jones, J. E., de Kok, J., Ozer, J., Pohlmann, T., Rasch, P., Skogen, M., Sorensen, J. T., 2002. NORTH SEA MODEL ADVECTION DISPERSION STUDY 2: Assessments of model variability, nomads-2: Final report. Tech. Rep. MAS3-CT98-0163, Commission of the European Countries, Brussel, Belgium.

Rodi, W., 1980. Turbulence models and their application in hydraulics. Tech. rep., Int. Assoc. for Hydraul. Res., Delft, The Netherlands.

Schmidt, M., Seifert, T., Lass, H. U., Fennel, W., 1998. Patterns of salt propagation in the southwestern Baltic Sea. Dt. Hydrogr. Z. 50, 345–364.

Schrum, C., Janssen, F., Hübner, U., 2000. Recent climate modelling in North Sea and Baltic Sea, Part A: Model description and validation. Tech. Rep. 37, Ber. Zentrum f. Meeres- u. Klimaforschung, Hamburg, Germany.

Seifert, T., Kayser, B., 1995. A high resolution spherical grid topography of the Baltic Sea. Meereswiss. Ber., Warnemünde 9, 73–88.

Simpson, J. H., Burchard, H., Fisher, N. R., Rippeth, T. P., 2002. The semidiurnal cycle of dissipation in a ROFI: model-measurement comparisons. Cont. Shelf Res. 22, 1615–1628.

Stips, A., Bolding, K., Pohlmann, T., Burchard, H., 2004. Simulating the temporal and spatial dynamics of the North Sea using the new model GETM (general estuarine transport model). Ocean Dynamics 54, 266–283.

Stips, A., Burchard, H., Bolding, K., Eifler, W., 2002. Modelling of convective turbulence with a two-equation k-ε turbulence closure scheme. Ocean Dynamics 52, 153–168.

Umlauf, L., Burchard, H., 2003. A generic length-scale equation for geophysical turbulence models. Journal Marine Research 61, 235–265.

Weiergang, J., Jønsson, M. (Eds.), 1996. DYNOCS technical data report. Danish Hydraulic Institute, Hørsholm, Denmark.

Zalezak, S. T., 1979. Fully multidimensional flux-corrected transport algorithms for fluids. J. Computat. Phys. 31, 335–362.

Mission of the JRC

The mission of the JRC is to provide customer-driven scientific and technical support for the conception, development, implementation and monitoring of EU policies. As a service of the European Commission, the JRC functions as a reference centre of science and technology for the Union. Close to the policy-making process, it serves the common interest of the Member States, while being independent of special interests, whether private or national.

EUROPEAN COMMISSION
DIRECTORATE-GENERAL
Joint Research Centre